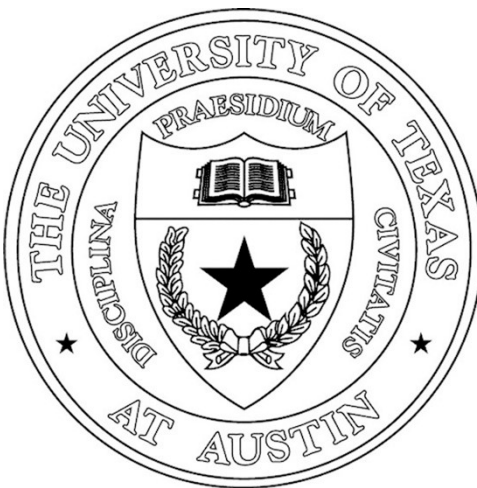


Design and Analysis of a Hybrid Rocket Engine

Submitted to:

Eric Richter, Propulsion Lead
Longhorn Rocketry Association
Austin, TX



Prepared by:

Shane Mathew
Mahdi Koubaa
Akshay Kulkarni, Team Leader
Daniel Teal

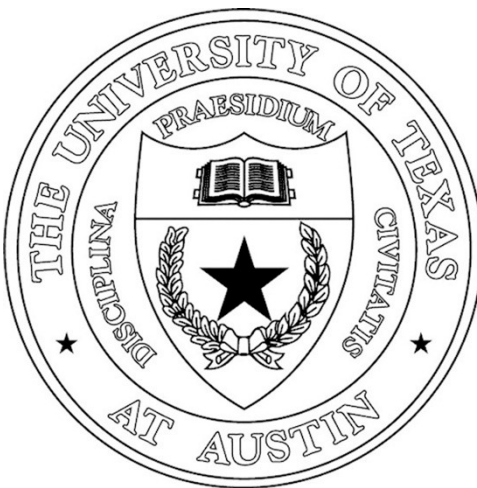
Mechanical Engineering Design Project Program
The University of Texas at Austin
Austin, Texas

Spring 2019

Design and Analysis of a Hybrid Rocket Engine

Submitted to:

Eric Richter, Propulsion Lead
Longhorn Rocketry Association
Austin, TX



Prepared by:

Shane Mathew
Mahdi Koubaa
Akshay Kulkarni, Team Leader
Daniel Teal

Mechanical Engineering Design Project Program
The University of Texas at Austin
Austin, Texas

Spring 2019

ACKNOWLEDGEMENTS

We would like to thank Eric Richter, Joe Do, Shawn Victor, and the rest of the LRA for providing the inspiration for this project. Thanks also to Dr. Bogard for his assistance and patience with our occasionally inane questions. Finally, thanks to Dr. Crawford, our TA, Dipankar, and the K project team for accepting this project and running the course.

TABLE OF CONTENTS

Acknowledgements.....	i
Table of Contents	iii
List of Figures	v
List of Tables	vii
Executive Summary	ix
1 INTRODUCTION.....	1
1.1 Sponsor Introduction and Context.....	1
1.2 Faculty Advisor Introduction	2
1.3 Team Introduction.....	2
1.4 Project Summary	3
1.5 Project Goals	4
1.6 Project Specification	6
1.6.1 Specification Sheet	8
2 ALTERNATIVE DESIGNS	9
3 PROJECT SOLUTION	13
3.1 Fuel Grain	13
3.1.1 Fuel Grain Manufacturing	13
3.1.2 Fuel Grain Regression Calculator	16
3.1.3 Fuel Grain Conclusions	17
3.2 Finite Element Analysis	18
3.2.1 Engine Case Analysis	18
3.2.2 Bolt Loading.....	21
3.2.3 Bolted Joint Analysis.....	23
3.2.4 Nitrous Oxide Flow Analysis	26
3.3 Rocket Geometry.....	29
3.3.1 Nozzle Sizing	29
3.3.2 Determining Nozzle Geometry	32
3.3.3 Combustion Chamber Sizing	34
3.3.4 Combustion Chamber Length.....	34
3.4 Thermal Analysis	37
3.5 Thermal Model Calculations	39
3.6 Thermal Protective Materials Study.....	42
3.7 Financial Overview	45
3.8 Test Site Details	47
4 CONCLUSIONS AND RECOMMENDATIONS	48
References	49
Appendix A Gantt Chart	A-1
Appendix B Patent Search.....	B-1
B.1 Fuel Grain	B-1
B.2 Thermal Protective Material	B-3
Appendix C Fuel Grain Test Procedures.....	C-1
C.0.1 Fuel Grain Fabrication Test Plan–Control	C-1

C.0.2	Fuel Grain Casting Test Plan—Shaker Table	C-3
C.0.3	Fuel Grain Casting Test Plan—Vacuum.....	C-7
Appendix D	Structural FEA	D-1
Appendix E	Fuel Grain Regression Calculator Results	E-1
Appendix F	Fluid Geometry	F-1
F.1	Nozzle Output Results	F-1

LIST OF FIGURES

Figure 2.1 The analysis of various sections of the engine required different approaches.....	10
Figure 2.2 A mind map of rocket failure modes and analysis techniques that can be used to address each. For example, a transient thermal simulation can be used to assure the engine chamber does not melt.	11
Figure 2.3 Assorted methods may be used to cool the engine.	12
Figure 3.1 Example thrust variance due to presence of bubbles in fuel grain[1]. .	13
Figure 3.2 Fuel grain being cast into a PVC mold.	14
Figure 3.3 The control fuel grain mold. Note the slightly lighter colored bubbles present throughout the cross-section.	15
Figure 3.4 The vacuum fuel grain mold, virtually bubble-free on the bottom.	16
Figure 3.5 An example cross-section of the fuel grain. This image represents a four-by-four inch square area; the grain itself is a 4 in. diameter cylinder. Running the simulator with this image, one of the examples of E, reveals a nearly constant but still suboptimal thrust curve.	17
Figure 3.6 Loading on Injector section of engine (CAD model courtesy of LRA)	19
Figure 3.7 Results of Injector FEA Analysis (CAD model courtesy of LRA)	20
Figure 3.8 Loading of Nozzle Section of the Engine (CAD model courtesy of LRA)	21
Figure 3.9 Results of Nozzle FEA Analysis (CAD model courtesy of LRA)	21
Figure 3.10 Bolt Calculator with various inputs	25
Figure 3.11 Bolt Calculator with stiffness and stress values.....	25
Figure 3.12 Injector Transient 2 Phase Flow at steady state	26
Figure 3.13 1-dimensional 2-phased flow calculator.	28
Figure 3.14 Dimensions of Sizing a Conical Nozzle [2].....	32
Figure 3.15 Nozzle Entry and Exit angles based on expansion ratio [2]	33
Figure 3.16 Dimensions of Sizing a Nozzle [2]	33
Figure 3.17 Correlation of Combustion Area to Throat Area [3]	35
Figure 3.18 Correlation of Chamber Length to Throat Diameter [4]	35
Figure 3.19 Dimensions of the combustion chamber [2]	36
Figure 3.20 1-dimensional thermal model [2].....	37
Figure 3.21 Case temperature increase over time	37
Figure 3.22 Heat flow into case over total operating time	38
Figure A.1 The current project schedule, as a Gantt chart	A-1
Figure B.1 An additively manufactured fuel grain. Fuel is laid down in paths (12) as is typical for FDM printing processes, and ripples in these paths (14) form channels through the grain (16) for faster combustion.	B-2
Figure B.2 An ablative material consisting of a hexagonal truss reinforcement (12), of fiberglass or similar (nonmetallic) material, and an ablative material (14) filling the interior of the hexes (13) of the truss.	B-4
Figure C.1 Cut and ground PVC piping in proper mold orientations	C-2

Figure C.2 Hardened Fuel grain control mold, bubbles are present as the white regions, where clear golden regions are absent of bubbles (marked in red) ...	C-3
Figure C.3 test stand setup of homemade shaker table.....	C-5
Figure C.4 Cut and ground PVC piping in proper mold orientations	C-6
Figure C.5 Cross-section of HTPB exposing bubbles (lighter areas)	C-7
Figure C.6 Cut and ground PVC piping in proper mold orientations (same as shaker test piping).....	C-9
Figure D.1 Final Case Temperature Distribution on outer case surface	D-1
Figure D.2 Case Loading Conditions for Transient Structural Analysis.	D-2
Figure D.3 Final structural coupled result.	D-3
Figure D.4 Whole case structural coupled result	D-4
Figure D.5 Case Deformation.	D-5
Figure D.6 Case Temperature Distribution at t = 0s.	D-6
Figure D.7 Case Temperature Distribution at t = 1s.	D-7
Figure D.8 Case Temperature Distribution at t = 2s.	D-8
Figure D.9 Case Temperature Distribution at t = 3s.	D-9
Figure D.10 Case Temperature Distribution at t = 4s.	D-10
Figure D.11 Beginning at d = 0 in at the outer surface of the case and subsequent distributions are of 0.05 in increments until inner case is reached. Results from ANSYS simulation data	D-11
Figure D.12 The maximum temperature of the case over burn time from ANSYS simulation data.	D-12
Figure D.13 Nozzle retaining ring bolt loading (CAD model courtesy of LRA) ..	D-13
Figure D.14 Injector face bolt loading analysis (CAD model courtesy of LRA) ..	D-13
Figure D.15 Injector retaining ring loading (CAD model courtesy of LRA).....	D-13
Figure E.1 A sample analysis of a fuel grain. The original cross-section of the fuel grain is solid save for the yellow star in the center. During combustion, the fuel burns into the green, then blue areas, creating the perimeter and area curves shown on the right. Note the perimeter rises and falls at different times during combustion (the interior area, of course, always increases, as fuel does not un-combust).....	E-2
Figure E.2 A basic circle geometry. As expected, perimeter increases linearly with diameter increase, while area rises quadratically. This is useful as a test case and, indeed, the results of the calculator agree with geometric calculations for area and perimeter.	E-3
Figure E.3 A simple star of lines turns out to provide a near-constant perimeter. Tests (not shown here) imply the exact thrust curve depends on the width of each arm and the number of arms; fewer arms create a decreasing perimeter; more reverse the effect. A five-pointed star seems to be near the equilibrium for reasonable amounts of interior area. We do note that such thin channels in the original fuel grain require reasonably advanced manufacturing.	E-4

LIST OF TABLES

Table 1.1	Engine Specifications	8
Table 3.1	Nozzle Bolt Calculations.....	22
Table 3.2	Injector Face Bolt Calculations	22
Table 3.3	Injector Retaining Ring Bolt Calculations	22
Table 3.4	Estimated Losses for Small-Diameter Chambers [15].....	35
Table 3.5	Assorted matrix and filler materials for ablative composites.	43
Table 3.6	Important material properties of typical fiberglass. The glass transition temperature is used instead of melting point as the matrix resin combusts at some higher temperature. The exact properties vary widely between resin and glass fiber formulations.	44
Table 3.7	Important material properties of bulk calcium-stabilized zirconium oxide. Thin films may differ due to microstructure changes. Note that all properties are worse than fiberglass in exchange for a much higher melting point.....	45
Table 3.8	Project budget estimates	46
Table A.1	This current project schedule, as a table.....	A-2

EXECUTIVE SUMMARY

The University of Texas at Austin's rocketry club, the Longhorn Rocketry Association (LRA), is attempting to build a hybrid rocket engine to compete in the Spaceport America Cup, in which some of the world's best universities compete to launch rockets to 10,000 ft. To date, over the past 3-4 years, LRA has built an untested and overengineered (heavy) prototype, called Taurus I, and rough plans for a flight-weight engine, Taurus II. In order to build Taurus II, LRA will need to not only build but repeatedly test the engine on a grounded test stand to determine and optimize their characteristics. The better the engine is theoretically understood, however, the less testing is necessary. Thus, we optimized and analyzed the Taurus II designs to both improve its characteristics and provide theoretical performance behavior to match future empirical test data, putting LRA in a good position to manufacture the engine and mount it in a rocket for the summer 2020 SAC. The plan is to improve thrust wherever possible, as a surplus of thrust is easily fixed by removing fuel, but a deficit is impossible to correct.

The Taurus II hybrid engine is powered by self-pressurized nitrous oxide, which, after passing through an injector plate, reacts with a solid fuel grain before expanding and passing out a nozzle. We were able to optimize most parts of this engine:

The fuel grain is cast into a suitable mold, but often contains up to 10% volume of air bubbles, which make the engine thrust nonuniform and reduce energy density. By casting the fuel in a vacuum chamber, we were able to remove all visible bubbles from the grain. The geometry of the grain is even more important: the surface area of its inner channel, which the oxidizing N_2O flows through, determines the reaction rate. This surface area should remain constant for constant thrust even though the fuel is constantly burning away. We programmed a fuel grain regression rate simulator that can determine how this surface area changes over time. Using this to optimize the fuel grain channel shape, we found geometries that can reduce thrust uniformity by up to 7x or, at the cost of uniformity, provide up to (an optimistic) 50% more thrust, which can also be traded for a 3.4lb weight savings, 7% of the total engine weight. These numbers should be empirically verified.

Next, we simulated the structure of the engine under expected thermal and mechanical loadings. We found LRA's proposed engine casing satisfied the safety factor of 2 required by the SAC with a slightly thinner ablative (heat protection) inner layer. We also verified the strength of the bolts used to assemble the engine. Finally, we analyzed the fluid flow through the engine. CFD determined the injector nozzles will successfully vaporize all N_2O and we optimized the nozzle and combustion chamber sizes. Most importantly, changing the oxidizer-to-fuel ratio, achieved by increasing the oxidizer mass flow rate, gives up to about 16% more thrust.

All these results will now be given to LRA. In addition, simplified calculators—the fuel grain regression simulator, a 1D heat transfer network, a bolt strength calculator, and nozzle and combustion chamber calculators—were developed so that LRA can further optimize Taurus II or future engines if they choose. We believe these results, which, if all implemented and tested, may increase empirical thrust by over 50%, are significant, and, if nothing else, LRA has more confidence in its engine design and can begin manufacturing to test the Taurus II hybrid engine before the summer 2020 SAC competition.

1 INTRODUCTION

1.1 Sponsor Introduction and Context

The Longhorn Rocketry Association (LRA) is the University of Texas at Austin's premier student rocketry club. LRA comprises a number of engineering undergraduates who build and test small to medium size rockets for experience, delight, certifications, and competitions. LRA's largest annual efforts are put toward the construction of a rocket for the Spaceport America Cup (SAC), in which university rocketry teams attempt to launch rockets to precisely 10,000 feet. Teams that compete in the SAC represent some of the best universities in America and worldwide.

Despite years of experience, however, the LRA has not yet risen to the heights of many other teams who build more technically complex rockets. Rockets are powered by engines, which typically fall into one of three types:

- Solid rocket engines, in which a fuel and oxidizer mixture are cast into a solid block. These engines have little to no control and cannot be quenched once lit, but are cheap and robust, commonly being found in model rockets. All of LRA's previously launched rocket engines are of this type.
- Liquid fuel rocket engines, in which the fuel and oxidizer are both cryogenic liquids, pumped to a combustion chamber before ignition. These engines, commonly used by commercial operators, are technically complex but fully controllable and refuelable.
- Hybrid rocket engines, finally, are a combination of the above two. A liquid or gaseous oxidizer is fed through a solid rocket fuel block, inside which combustion occurs. This engine may be throttled but its fuel, once spent, must be replaced in its entirety. However, the combination of simplicity and greater control makes this a sweet spot for high-powered amateur rocketry.

In particular, LRA has never tested, let alone flown, a hybrid rocket engine, unlike teams from many other universities (liquid fuel engines are too complex for all but the most advanced programs). In fact, LRA has never hot-fired any custom built engine. Thus, over the past couple of years, LRA has been working toward a hybrid rocket engine. The first prototype, Taurus I, has been completed as a test bed engine for learning and characterization of the system, but has not been tested. Taurus II, a flight-weight version intended to be mounted within a rocket, has been sketched out but is unoptimized.

Our team has performed the final analysis and optimization of Taurus II. Our goal is to provide LRA with the analysis tools and necessary resources to optimize the current design while shortening the design cycle for future iterations. Hopefully, the rocket engine will be manufactured and mounted in a rocket for the summer 2020 SAC. Funding was provided by LRA. Our contact within LRA is the head of their propulsion team, Eric Richter. We worked with Eric and his team for duration of this project.

1.2 Faculty Advisor Introduction

Our faculty advisor is Dr. David Bogard, who holds the Baker Hughes Incorporated Centennial Professorship in Mechanical Engineering and is the associate department chair of the Walker Department of Mechanical Engineering. Dr. Bogard earned his Ph.D. from Purdue in 1982, and now researches turbine blade cooling and associated fluid mechanics. His aerospace expertise includes building his own airplane.

Dr. Bogard has helped our group with thermal management calculations and design of the oxidizer 2-phase flow through the injector. He has been instrumental in verifying our analysis approach and troubleshooting our results.

1.3 Team Introduction

We, the team, are four mechanical engineering seniors at the University of Texas at Austin. We are all apprentices of different fields of the discipline, creating a large knowledge pool to draw from.

- Shane Mathew has worked previously at assorted companies in the oil & gas industry. He knows his way around piping and is very aware of the safety precautions and standard procedures used to reduce accident rates in high-stakes situations. Shane analyzed bolt strengths.
- Mahdi Koubaa is an expert machinist. He has researched internal combustion engines and enjoys working with automobiles. Mahdi improved the solid-fuel casting process.
- Akshay Kulkarni is our rocketry expert. He has studied rocket engine combustion for a number of years, including a stint at SpaceX. Akshay's passion is computational fluid dynamics; he has optimized the dimensions of assorted fluid chambers in addition to running an FEA of the engine under thermal loading.
- Daniel Teal studies robotics and nanotechnology. In the pursuit of creating micron-scale functional machines, he has gained an understanding of electronic material structure and system design. He optimized material choices for the engine and created a fuel grain regression calculator.

1.4 Project Summary

Our semester goal was to analyze and optimize a hybrid rocket engine. Such an engine is more complex than common solid-fuel engines (although simpler than commercial liquid-fuel types) in order to allow the Longhorn Rocketry Association to participate in the Spaceport America Cup Hybrid Rockets category. While many amateurs have launched hybrid engine rockets, the Longhorn Rocket Association (LRA) has never successfully tested, let alone flown, such a hybrid rocket engine. Successful completion of this project would be a significant accomplishment.

We analyzed the flight weight engine (Taurus II) and worked toward a hot fire of the test bed engine (Taurus I). At the moment, LRA has a fully functional nitrous oxide feed system

("feed system"), a certified test stand ("thrust structure"), and a prototype untested hybrid engine. The current engine serves as a test bed for validating and procedural refinement. The engine design, using N2O/HTPB chemistry, was put under significant structural, thermal, and fluid analyses to ensure its proper operation. We also provided several areas for optimization, namely, the fuel grain, O/F ratio, and nozzle, which may be able to provide up to 50% more thrust, should LRA choose to do so.

Finally, we are providing LRA with a set of analysis tools they can use to tweak their design further. Because it is extraordinarily difficult to completely theoretically characterize a rocket engine, it is necessary to run multiple empirical tests to characterize an engine's performance before it can be used to reliably launch a rocket to a given height window, which is necessary to meet the SAC's exactly 10,000 ft goal (although other rocket subsystems, e.g., air brakes, can compensate somewhat for higher thrust). By using these analysis tools, in addition to optimizing the engine, LRA can better understand it, thereby requiring fewer test fires and saving weeks of work. With all this in place, we believe the engine is now in a position to be completed and tested on schedule for a future summer 2020 LRA rocket.

1.5 Project Goals

We accomplished the following goals over the course of this project, with the exception of a hot fire of Taurus I due to significant inclement weather.

1. Combustion chamber analysis and design
 - (a) Quantify and optimize chamber heat transfer and fluid flow
 - i. Perform coupled thermal analysis to determine minimum safety factor
 - ii. Determine minimum ablative and ceramic liner thickness
 - iii. Determine maximum case temperature at end of burn
 - (b) Design chamber to thermodynamic constraints while minimizing mass
 - i. Balance safety factor and manufacturability
 - (c) Research ablative materials and high-temperature ceramics for thermal management
 - i. Determine cost effective yet sustainable thermal management solution

2. Nozzle
 - (a) Optimize shape for efficient thrust with numerical analysis
 - (b) Determine minimum structural safety factor.
3. 2-Phase Flow Analysis
 - (a) Determine pressure drop required to maintain 2-phased mass flow rate
 - (b) Explore 2-phased flow through injector
4. Thermal Management Materials
 - (a) Determine and affordable yet sufficient thermal protective layer for chamber thermal protection
 - (b) Perform trade study between different commercially available materials
 - (c) Focus on rapid reusability and modularity of thermal protection
5. Bolt Stress Calculator
 - (a) Determine thermal influence on bolt strength
 - (b) Create a thorough and robust analysis tool for future bolt sizing considerations
6. Fuel Grain Regression Calculator
 - (a) Determine optimum fuel grain geometry based on fuel grain shapes
 - (b) Develop a rapid optimization tool for development of more intricate designs
7. Fuel Grain Manufacturing
 - (a) Develop and perfect fuel grain manufacturing procedure
 - (b) Experiment and validate different manufacturing methods for knowledge continuity
8. System Integration
 - (a) Compile all calculators and analysis tools into an engine design tool
 - (b) Complete leak checking and activation of LRA test stand - troubleshoot instrumentation and fluid systems
9. Testing
 - (a) Streamline test site procedures for cold flow and testing
 - (b) Hot fire Taurus I engine (stretch goal for project)

1.6 Project Specification

The specifications of our hybrid rocket engine, quantified in Table 1.1, are determined from organizational requirements, general execution rationale, and some basic calculations to ensure that the engine operates as intended. We organize the specifications into the following sections. The engine analysis targets ensure correct pressure and structural integrity. We fix chamber pressure of 500 psia as a compromise between high thrust and low thermal management requirements. A safety factor of 2 is required for all participants in the Spaceport America Cup 10,000 ft Hybrid category to ensure safe operation at the launch site, but minimizing the factor reduces weight. However, a larger safety factor provides a healthy margin for the strength of components being used; since bolts and threads can be subject to dynamic loading and thermal fatigue and contribute relatively little to the total mass, we assign them a higher minimum safety factor of 5. We'll design for pressure drop of 100 psia across the injector to ensure the injector flow is one direction; this necessitates a pressure of 600 psia before the injector orifices. Finally, keeping the casing temperature to 300°F ensures that thermal stresses are far below that which would deform and weaken the metal. Inside the chamber, the thermal protective material ("ablative", whether it ablates or not) must withstand the combustion temperature of 3200°F to prevent heat transfer to the casing, while the fuel grain mold must exhibit less than 10% of the surface area in air bubbles within the grain, to make a uniform thrust profile. Nozzle requirements are in place to ensure maximum thrust, efficiency, safety, and expansion ratio. The thrust value was calculated using an open source trajectory simulation software called OpenRocket. The equivalent solid rocket motor was used in the simulation, with an input of mass, rocket geometry, thrust, and various other parameters inputted in order to achieve our desired height. The Isp, efficiency of a rocket engine, is given a 200s + requirement to ensure the minimum amount of fuel is required to reach the highest possible altitude. A safety factor of 2 for the nozzle is again used as a standard structural safety factor. Finally, the test stand is designed to safely test the rocket in a reasonable amount of time. With that in mind, a maximum

time of 8 hours per test is critical to ensure testing concludes within a day. Due to the fact that the rocket will only burn for a few seconds, the high data sampling rate of at least 60 hz would give us plenty of data points to analyze. Finally, the stand must safely flow at least 3.63 lbm/s of oxidizer. This is the targeted oxidizer flow rate from the N₂O pressure tank. This is necessary in order to have the rocket engine at the optimal air/fuel ratio of 6.3 resulting in an optimal burn. Lastly, our project is a student built rocket engine so cost must not exceed \$1000.

1.6.1 Specification Sheet

Table 1.1. Engine Specifications

D/W	Metric	Value	Units	Test Method
Combustion Chamber Analysis				
D	sustain chamber pressure	500	psia	tank calculator
D	structural minimum safety factor	2	-	FEA
D	bolt minimum safety factor	5	-	bolt calculator
D	injector 2-phase flow drop	100	psia	calculator
D	maximum case temperature	300	F	thermal FEA
D	optimize flow coefficient	TBD	-	empirical testing
D	constant fuel grain perimeter	3.25	in	regression simulator
Ablative Requirements				
D	minimum ceramic melting point	3000	F	material choice
D	minimize coating stress	TBD	psia	empirical testing
Fuel Grain				
D	minimize grain bubbles	10	% area	image processing
D	grain template removal	1	lbf	force gauge
Nozzle				
D	thrust value	730	lbf	nozzle calculator
D	engine efficiency (Isp)	200+	s	nozzle calculator
D	minimize safety factor	2	-	FEA
D	target expansion ratio	5.26	-	nozzle calculator
D	nozzle length (bell nozzle)	80	%	nozzle calculator
Manufacturing				
D	meet budget	1000	\$	accounting
Test Stand				
D	safely flow N ₂ O	3.63	lbm/s	cold flow
W	data sampling rate	60	Hz	testing
D	testing timeline	8	hour	dry run
D	site setup	4	hour	dry run
W	engine hotfire	4	hour	hot fire

2 ALTERNATIVE DESIGNS

We began this project with a series of meetings with the LRA leadership. Based on these talks, we determined the components that required the most attention for analysis. The issues identified were as follows in Fig. 2.1:

1. Fuel Grain Manufacturing—inconsistencies in the manufacturing process caused air bubbles to form causing non-uniform combustion
2. Fuel Grain Regression Simulation—maintaining a constant perimeter of the fuel grain is required to maintain a constant thrust
3. Ablative Selection—no thermal analysis had been performed on the engine
4. Chamber & Nozzle Sizing—sizing had been done based on general rules of thumb and not according to available empirical correlations
5. Injector testing—characterization of the flow coefficient has not been performed
6. Bolt Selection—no analysis had been performed for bolt sizing with thermal stresses
7. Testing Standard Operating Procedures—testing procedures require significant improvement in order to conduct operations safely
8. Feed System—redesign of the feed system required to minimize 2 phase flow

Fig. 2.1 labels a drawing of the engine with assorted parts that could be optimized, each in a different way. To determine how to direct our analysis efforts, we created the mind-map shown in Fig. 2.2. We also put some creativity into choosing alternatives for thermal protection for the combustion chamber, shown in Fig. 2.3.

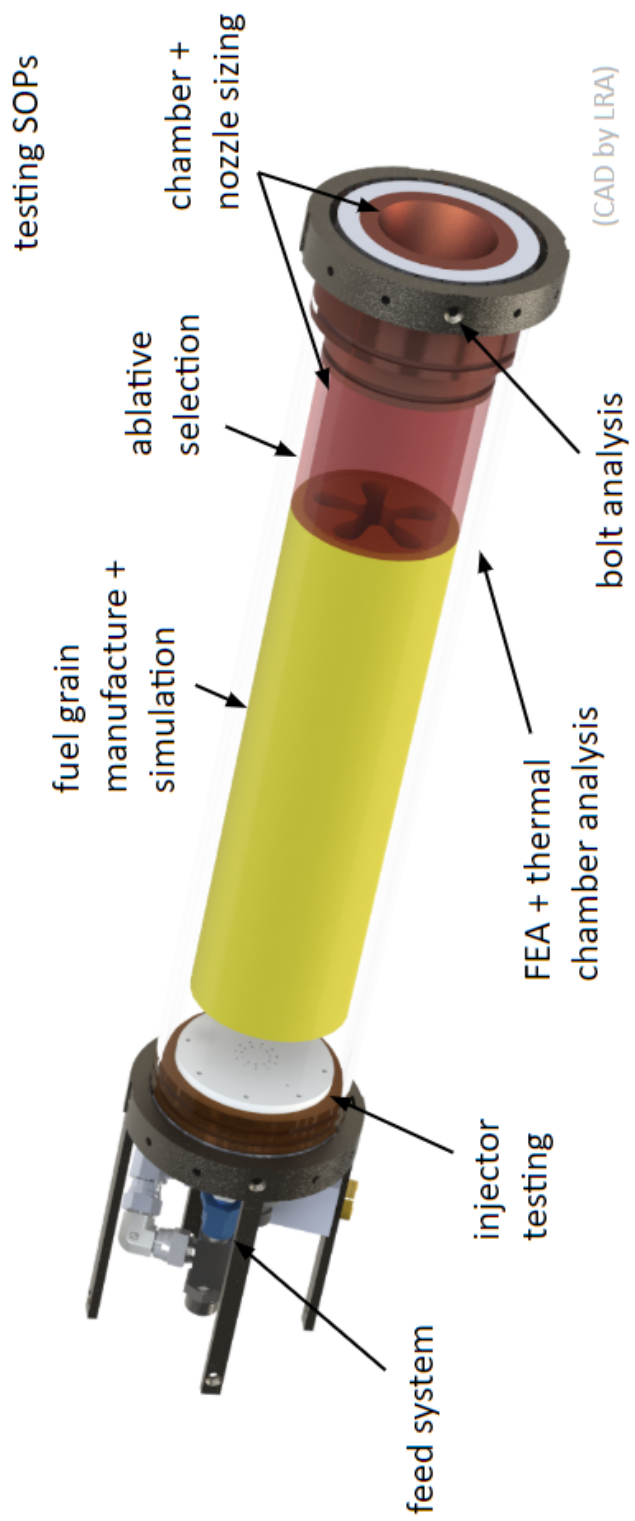


Figure 2.1. The analysis of various sections of the engine required different approaches.

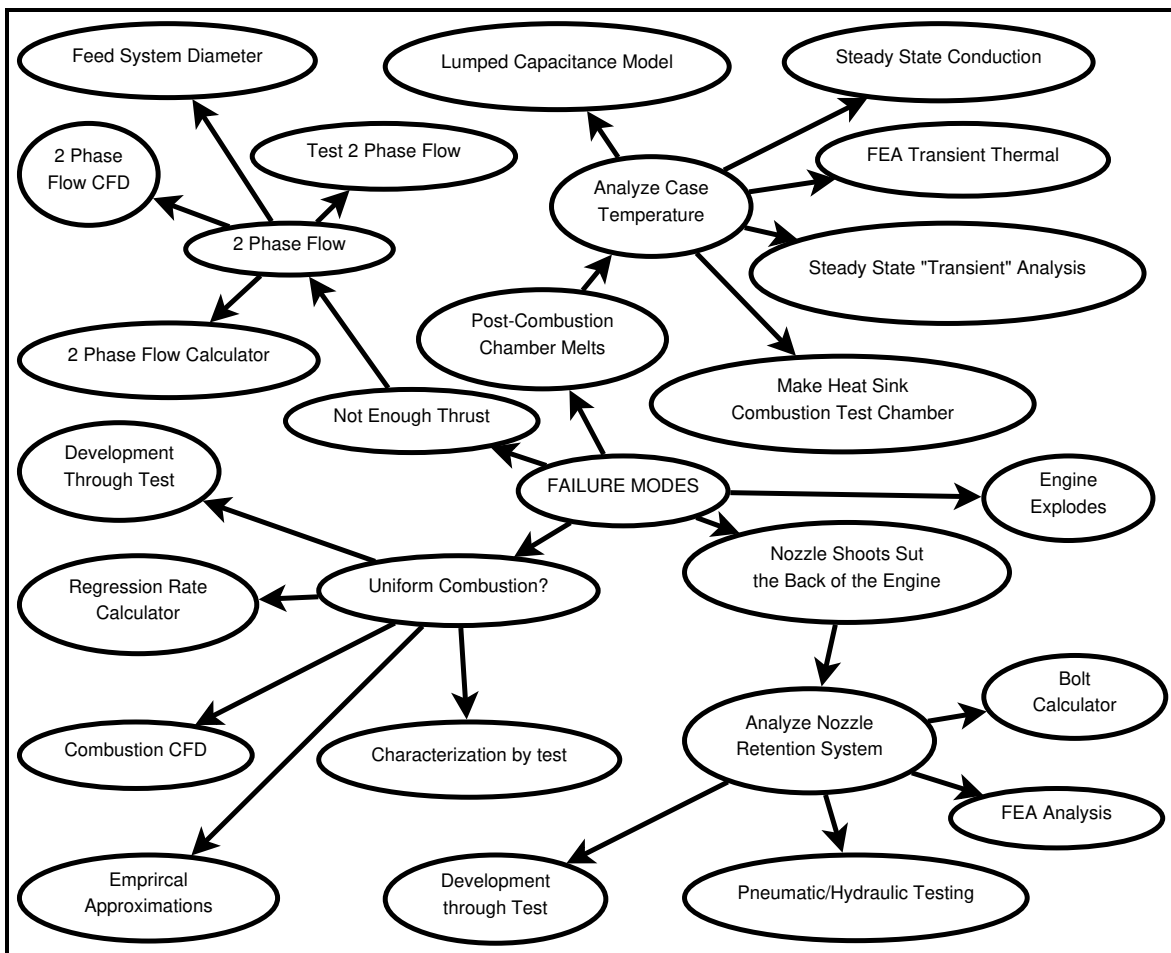


Figure 2.2. A mind map of rocket failure modes and analysis techniques that can be used to address each. For example, a transient thermal simulation can be used to assure the engine chamber does not melt.

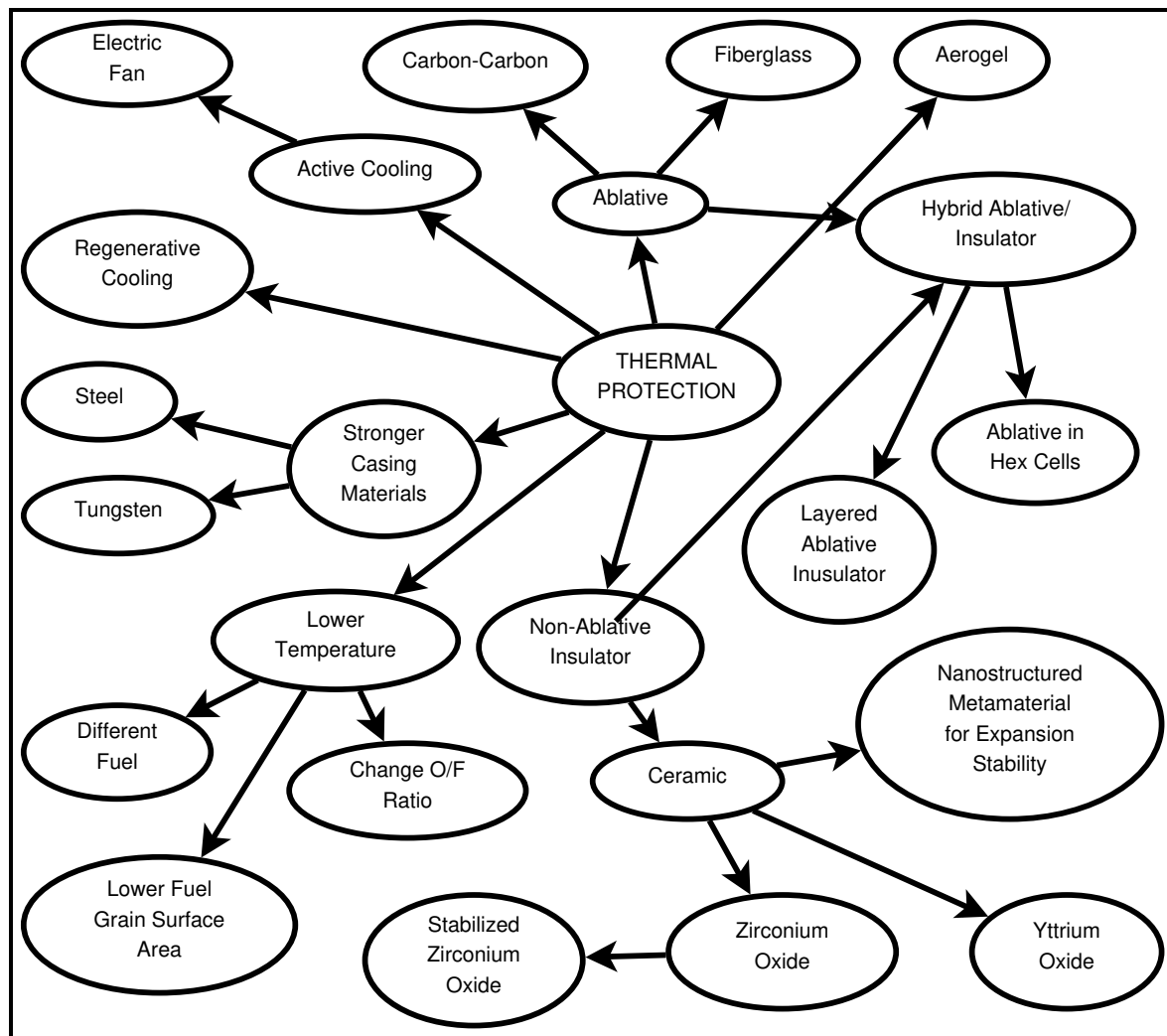


Figure 2.3. Assorted methods may be used to cool the engine.

3 PROJECT SOLUTION

The bulk of our project became the analysis of multiple parts of the Taurus II rocket engine. In this section, we detail each analysis. These analyses include manufacturing the fuel grain to minimize bubbles, simulating its regression, ensuring neither the engine casing nor its bolts rupture or break under expected thermal and mechanical loads, and optimizing the fuel flow through the injector, post-combustion chamber, and nozzle.

3.1 Fuel Grain

3.1.1 Fuel Grain Manufacturing

The solid fuel grain is an integral part of the hybrid rocket engine. The texture of the fuel grain should be consistent and smooth in order to have a predictable and stable burn. A typical problem with solid rocket fuel is the presence of air bubbles. As the rocket fuel burns from the inner surface, air bubbles burned will cause a spike in surface area, which subsides as the grain burns past these bubbles. Since thrust is directly related to perimeter, this also causes spikes in the thrust curve. Air bubbles found in the fuel grain also cause a density that is far lower than theoretical, lowering energy density. Experimental Fuel grains are estimated to have a grain density of between 90-98 percent of a bubble free theoretical grain [1]. Removing the uncertainty from this variable will create a rocket that is more precise, reducing the need to perform multiple tests. This phenomenon is shown in 3.1.

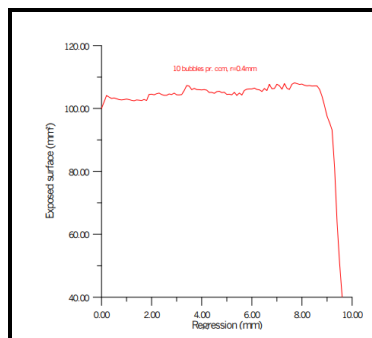


Figure 3.1. Example thrust variance due to presence of bubbles in fuel grain[1].

Unfortunately, the current fuel grain pouring procedures generate these air bubbles. To

minimize or reduce this effect, we tested variations on the standard fuel grain manufacturing procedure. In particular, mixing ratios, heat of mold, pressure surrounding mold, and other factors can all affect the formation of air pockets.

The grain is made up of solid HTPB (Hydroxyl-terminated polybutadiene) mixed with a binding agent. The HTPB must be cast and hardened into a solid grain with an even consistency, however it commonly forms bubbles in the grain. The presence of air bubbles will cause an inconsistent burn, and may even cause an unsafe explosion [1]. In order to counteract this, tests are being undertaken in order to cast a grain without any air bubbles present.

As is important in any experiment, first, a control mold was poured. As expected, excessive amounts of air bubbles formed in this control mold. In order to produce a seamless grain, a simple mold is created using PVC pipes and cardboard (see Fig. 3.3). The pouring process uses 86 percent HTPB (Hydroxyl-terminated polybutadiene) and 14 percent binder compound. Typically, a mixing time of 60 seconds and a cure time of 48 hours is required. The complete test plan for the control mold is documented in Appendix C.



Figure 3.2. Fuel grain being cast into a PVC mold.

Next, three additional tests are undertaken, detailed in Appendix C. The first test involves a shaker table which is created using a reciprocating saw, wood, and wood clamps. First, the mold is poured identically to the control, and the mold is shaken for 30 minutes, then set to harden. This did not have a significant effect on the air pockets. For the second test, because most bubbles seem to be created during mixing, the fuel is poured and mixed



Figure 3.3. The control fuel grain mold. Note the slightly lighter colored bubbles present throughout the cross-section.

for only a short amount of time. The bubbles started forming during the mixing procedure. This produced a grain which was virtually bubble free, however this mold did not completely harden, and became increasingly sticky. The mixture was not homogeneous, which demonstrates a trade off with air pockets and homogeneity, something that could be optimized through altering mixing time. Finally, the third test is poured and placed in a vacuum chamber, with the expectation that the fuel bubbles will be extracted in the low pressure environment. This resulted in a higher bubble density on the exposed surface of the grain, but, when the grain was cut, it could be clearly seen that the bubbles indeed rose to the surface. The lower half of the grain held very few bubbles (Fig. 3.5).

Lastly, because all sample fuel grains are shorter than the grains to be used in the rocket, a test was performed to determine the effect of fuel grain height on bubble density (see Appendix C for details). An identical test using the vacuum chamber was undertaken with a short grain and a tall grain in order to observe how the bubble density changed throughout differing heights. The relationship of bubble concentration and height from the top of the cylinder was seen. In other words, regardless of the height of a bubble grain, we can estimate the grain width that needs to be chopped off. The fuel grain bubbles present on the surface of the mold might be misrepresented. As the bubbles propagate to the surface



Figure 3.4. The vacuum fuel grain mold, virtually bubble-free on the bottom.

and diffuse into the air, it is probable that the uppermost surface contains a high density of bubbles whereas the central and lower regions of the grain may have a lower density of bubbles. For future analysis, taking a clean slice can provide a better idea of the overall bubble density of the fuel grain. Bubble density can be analyzed by looking qualitatively at the grain texture. This is supplemented by quantitatively counting the amount of air bubbles present, and comparing it to other grains.

3.1.2 Fuel Grain Regression Calculator

In order to maintain a desired thrust curve, the combustion in the rocket engine must happen at a particular rate. Taurus II is being designed for a constant thrust over four seconds, but there exist other possibilities. This thrust curve, whatever shape it is, is determined by the geometry of the fuel grain. The combustion rate is proportional to the surface area of the interior of the fuel grain, but as combustion progresses, the fuel grain burns away—“regresses”—changing its surface area. This makes designing for any particular thrust curve very challenging. We built a program to simulate fuel grain regression and calculate optimal geometry.

This regression rate calculator takes as input a 2D cross-section of the fuel grain, represented as a black-and-white PNG file, and uses image manipulation techniques to calculate how the shape will change as the fuel burns away (using the same method as [5]). At the

same time, the perimeter of the cross-section (which, when multiplied by length of the fuel grain, gives the surface area proportional to the combustion rate) and interior area (which affects the rocket chamber pressure) are calculated. It is assumed the regression rate is constant, which is a good approximation for constant mass flux and may be calculated via [6]. In reality, the regression rate will change with oxidizer-to-fuel ratio, chamber pressure, and other variables, and must be validated through empirical testing.

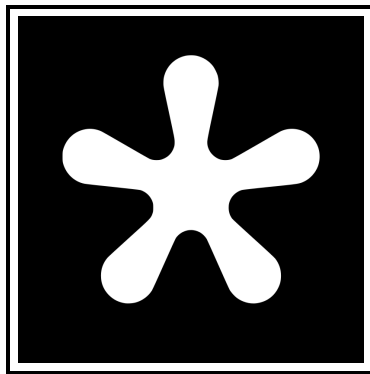


Figure 3.5. An example cross-section of the fuel grain. This image represents a four-by-four inch square area; the grain itself is a 4 in. diameter cylinder. Running the simulator with this image, one of the examples of E, reveals a nearly constant but still suboptimal thrust curve.

To find an optimal fuel grain shape, the user edits the cross-section image with a standard image editor (e.g., Krita, which has a symmetry painting mode useful for creating a uniform pattern), analyzes the image with this regression rate calculator, and compares the shape of the computed perimeter change to the desired thrust curve. This is repeated, at a rate of approximately one design each thirty seconds, until a sufficiently good result is found. We calculate the regression rates of some sample fuel grains in Appendix E with good results. It is possible to optimize for constant or very high thrust.

3.1.3 Fuel Grain Conclusions

The optimal fuel grain manufacturing technique uses a vacuum chamber mold. The fuel can be poured 2 inches taller than the desired grain height and cut to size, then transferred to the engine casing. To do this, a vacuum chamber and vacuum pump would need to

be purchased. For Taurus II, which has a final grain height of 14 in., we recommend a 17 in. tall vacuum chamber. A few other possibilities can be explored, such as using a vacuum chamber on the liquid HTPB before mixing, or creating a mixture in the presence of heat. It is also possible to further optimize bubbles through finding an optimal mixing time, reducing prior formations of bubbles.

The fuel grain simulator allows fast iteration of geometry designs. For Taurus II, we have found designs that can reduce thrust variability by up to 7% (with up to 20% more thrust) or, by neglecting the need for constant thrust (which can be offset by careful design of the rest of the rocket and its trajectory), a design that might increase thrust by up to 50% or save 3.4 lbm (7% of the engine total).

Finally, according to several patents (see Appendix B), ABS plastic, which is easily 3D printed, performs nearly as well as HTPB as hybrid rocket fuel. A sufficiently large printer, such as the Gigabot available in UT's Texas Inventionworks makerspace, could print a fuel grain with nearly arbitrary geometry, allowing for features as complex as twisted channels, which, if properly designed, can better mix the fuel and oxidizer [5]. However, each fuel grain would cost about \$60 and take multiple days to print, making this uneconomical compared to our HTPB grains.

3.2 Finite Element Analysis

Finite Element Analysis is a computational tool used by engineers in industry to develop and increase understanding of components prior to manufacture and testing. Running simulations is an affordable characterization method compared to testing expensive hardware. With reference to this project, Finite Element Analysis provides confidence in safe engine design and operation. This project utilizes ANSYS 19.0 structural and thermal simulation capabilities for analysis.

3.2.1 Engine Case Analysis

Modelling begins with initial sizing using fundamental equations and hand calculations. However, with modern computational tools and higher fidelity modelling, amateur

engineers can use Finite Element Analysis (FEA) to provide a deeper understanding into component behavior and allow for faster optimization. We have used FEA to structurally analyze Taurus II flight-weight engine [7].

Due to computational limitations, only relevant sections of the engine and analyzed local loading. As referenced in Fig. 3.6, there is two-way loading representing the incoming feed system pressure. At the top of the injector, the incoming tank pressure required to drive the 2 phase flow through the injector is 830 psi. Next, the pre-combustion chamber pressure at the bottom of the injector is loaded during the chamber pressure of 500 psi. The results show that the safety factor is around 7.5 shown in Fig. 3.7. We do not seek to mass optimize this section of the engine due to manufacturing and integration constraints.

This result was validated to ensure the solution was mesh independent. Essentially, we altered the mesh quality and observed the change in results. The overall differential in safety factor was below 5% rendering the result accurate.

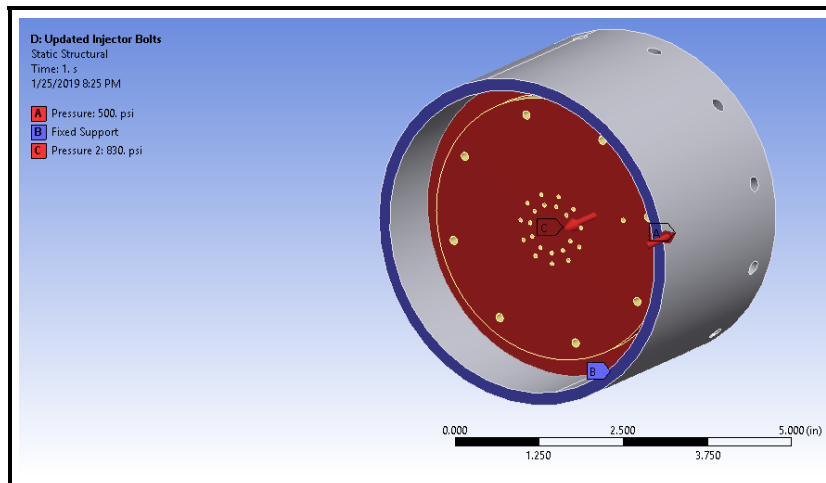


Figure 3.6. Loading on Injector section of engine (CAD model courtesy of LRA)

A similar analysis is carried out on the nozzle of the engine. The material property of the nozzle insert is changed to reflect the graphite material used. The nozzle is kept in place using a retaining ring and a series of bolted connections. Fig. 3.8 shows the chamber pressure loading on the exposed section of the nozzle to the chamber pressure of 500 psi. Fig. 3.9 indicates a safety factor of 5.5. A mesh independence study has been conducted

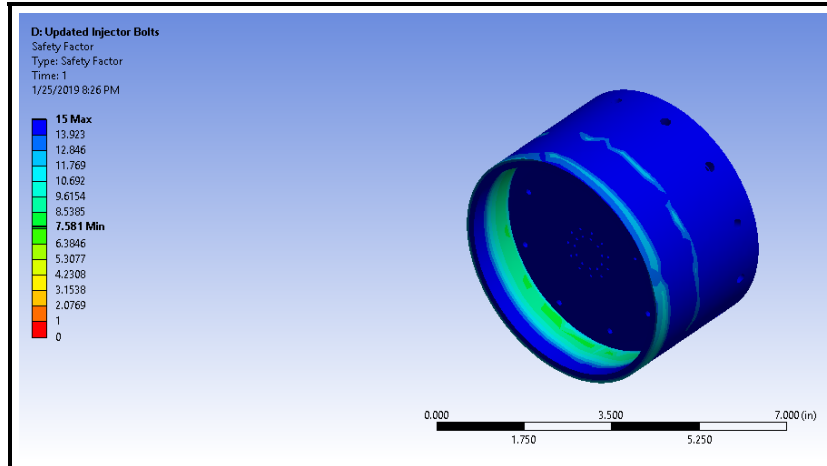


Figure 3.7. Results of Injector FEA Analysis (CAD model courtesy of LRA)

on this section of the simulation to validate results.

*Note: The thermal analysis for the nozzle was not performed as part of this project.

The rationale is the fact that the strength in graphite increase with temperature so room temperature structural analysis is the weakest structural state of the nozzle. Furthermore, the thermal conductivity of graphite is significantly low. Therefore, if the post-combustion chamber case section can survive flight, the nozzle case section can survive as well. However, analyzing this section of the engine may yield valuable insights.

*Note: Additionally, the exhaust plume of a rocket engine can be a significant source of radiative heating. As the plume becomes under-expanded, the flames move closer to the rocket body. This might cause weakening of the bolts in the retaining ring of the engine. This analysis must be complete before flight.

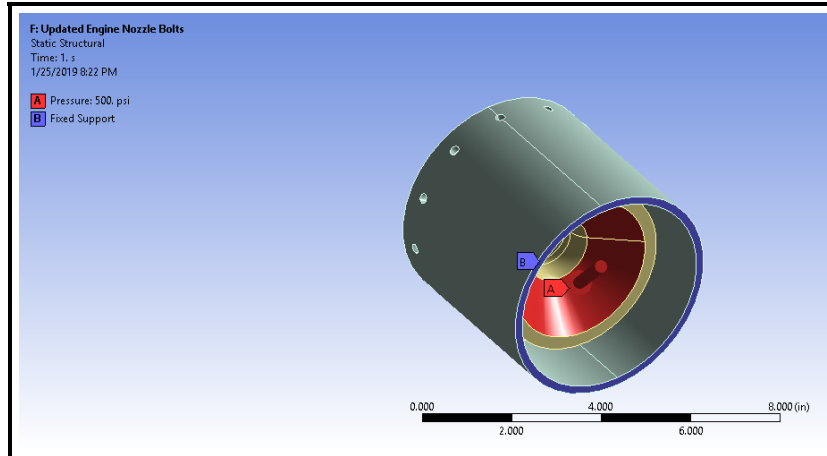


Figure 3.8. Loading of Nozzle Section of the Engine (CAD model courtesy of LRA)

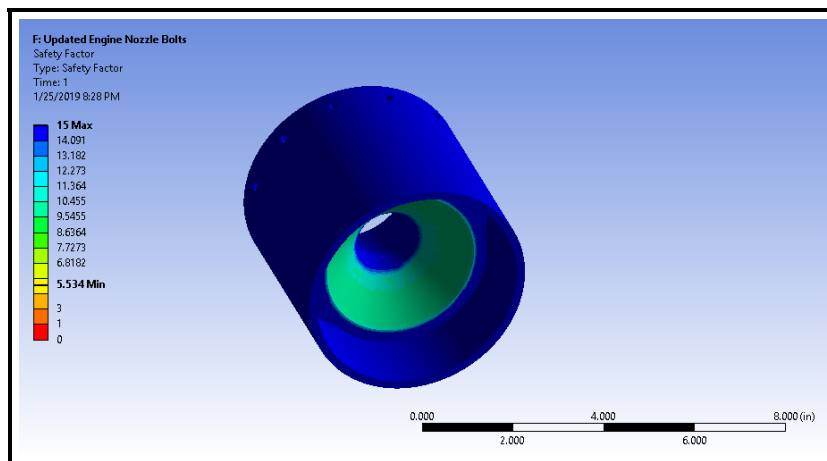


Figure 3.9. Results of Nozzle FEA Analysis (CAD model courtesy of LRA)

The FEA analysis shows that the injector mounting assembly and the nozzle housing assembly are overbuilt for the application. Even though the minimum safety factor is quite high, we will not be seeking to optimize for weight. The current dimensions will be kept intact for manufacturing and integration purposes.

3.2.2 Bolt Loading

Fig. D.13 shows the load experienced by each bolt due to loading in Fig. 3.8. The maximum bolt loading in shear is 304.25 lbf (see Table 3.1). Therefore, depending on the design and loading in future designs, LRA members will be able to size bolts accordingly. We have gotten recommendations to put the bolts in tension rather than shear. Bolts in

tension are stronger than in shear. However, this configuration is more manufacturable and a stronger bolt can be easily selected.

Table 3.1. Nozzle Bolt Calculations

Total Force X [lbf]	Total Force Y [lbf]	Total Force Z [lbf]	Total Force [lbf]
213.92	213.91	-32.432	304.25

Due to the loading described in Fig. 3.6, the maximum force exerted on the injector plate mounting bolts is 22.245 lbf in tension (see Table 3.2). This relatively small load is due to the differential pressure on either side of the injector being relatively small. Fig. D.14 describes the effective loading vector.

Table 3.2. Injector Face Bolt Calculations

Total Force X [lbf]	Total Force Y [lbf]	Total Force Z [lbf]	Total Force [lbf]
0.30185	7.4311	-20.96	22.245

Due to the loading described in Fig. 3.6, the maximum force exerted on the injector-engine case interface is 9.037 lbf in shear (see Table 3.3). This relatively small load is due to the differential pressure on either side of the injector being relatively small. Fig. D.15 describes the effective loading vector.

Table 3.3. Injector Retaining Ring Bolt Calculations

Total Force X [lbf]	Total Force Y [lbf]	Total Force Z [lbf]	Total Force [lbf]
-6.7906	-3.2266	-5.0143	9.037

3.2.3 Bolted Joint Analysis

Throughout the hotfire tests of the hybrid rocket, various factors will need to be considered in order to make sure the structural integrity and engine assembly remains in one piece. The engine casing, airframe, and overall structure will be held by clamping all components together. Bolts will be screwed into a retaining ring surrounding the structure and must be carefully assembled and designed to prevent relative motion in the individual components which could cause engine failure. The bolts currently designed to be installed are Stainless Steel and to be inserted through aluminum retaining rings and held within an aluminum block. The first effect to consider are vibrations caused by a hotfire test. During the four seconds of testing, the rocket will most likely undergo vibrations, which may loosen bolted joints throughout the engine. Higher strength steel inserts are recommended. These inserts lock onto the aluminum body and help to prevent thread distortion while maintaining bolted joint integrity. Four seconds is not a significant enough run time to loosen the bolts under normal circumstances. The steel inserts are used as a precautionary measure.

To understand the loads applied to the bolted joints, a bolt calculator is useful to help determine the overall forces affecting each bolt and whether or not they are capable to withstand all counteracting forces. The shear, tensile, and compressive forces are determined using equations derived from ASME standards and allow us to calculate the torque required to safely fasten the bolted joints to maintain engine retention [8][9].

Using basic bolt and material characteristics such as nominal diameter and yield strength as seen in Fig. 3.10, the program calculates important geometries of the internal and external threads and determines the minimum torque and preload values to fasten the bolts in place while taking into consideration the torque and friction coefficients between the mating surfaces. Next, the bolt and overall joint stiffness values are determined by approximating the components as springs in a grip. Equation 3.1 below is used to calculate the overall stiffness of the joint. It uses the elastic modulus of the bolt material, minor diameter (d), major diameter (D), and thickness of the various frustums within the joint as well as

the angle of the threads (estimated to be 30 degrees).

$$k_{fr} = \frac{\pi Ed \tan \alpha}{\ln \left[\frac{(2t \tan \alpha + D - d)(D + d)}{(2t \tan \alpha + D + d)(D - d)} \right]} \quad (3.1)$$

Once the overall stiffness of the joint is confirmed, the joint constant can be determined to understand how the bolt load acts against the applied load as seen in Equation 3.2.

$$C = \frac{k_{bolt}}{k_{bolt} + k_{grip}} \quad (3.2)$$

This can be used to determine the amount of force necessary to separate the joint as well as the safety factor. Using this information and combining the various stresses found in the system due to shear and tension, the Von Mises Stress equation below in Equation 3.3 can be used to iteratively find the factor of safety for the bolted joint. It uses the shear stress, tensile stress, bending stress, and the load factor to determine the Von Mises stress and altering the load factor value (n) can lead you to a Von Mises stress value that equals the allowable stress. An example iteration can be seen in Fig. 3.11.

$$\sigma_{VM} = \sqrt{[\sigma_{PL} + n(\sigma_t + \sigma_{bnd})]^2 + 3(n\tau_{sh})^2} \quad (3.3)$$

Finally, the bolt calculator considers both the internal and external threading and calculates the factor of safety regarding the shear forces. Using this calculator, the 4-40 Grade 8 Hex Bolts are strong enough to withstand the operating forces.

The last major point to consider would be the thermal effects on all the bolts and threads. The four-second exposure during the test will only raise the temperature of the aluminum block inside the engine and the retaining rings to about 200 degrees Fahrenheit which is not a significant change considering that the melting point of Aluminum 6061 is around 1200-degrees Fahrenheit. Aluminum 6061-T6 loses about 50% of its Ultimate Tensile and Yield strength around 600°F and thus a service temperature of about 200°F for about four seconds will not have any significant effect on the structural integrity.

Bolt Characteristics			Bolt Geometry		
Pitch	P	0.025	External Thread, Minor Diameter	Dmext	0.07952
TPI	TPI	40	External Thread, Pitch Diameter	Dpext	0.09576
Nominal Diameter	Dnom	0.112	Internal Thread, Minor Diameter	Dmint	0.08494
Length of Bolt	L	0.25	Internal Thread, Pitch Diameter	Dpint	0.09576
Tensile Yield Strength	Sty	150000	External Thread Nominal Area	Anom	0.00985
Elastic Modulus of Bolt	E	3E+07	External Thread Tensile Stress Area At	At	0.00603
			External Thread Minor Area	Am	0.00497
Preload					
			Preload Value	Fpl	579.149
Torque					
			Torque	T	13.2922
			Torque Coefficient	Kt	0.20492
			Mean Thread Radius	rt	0.04788
			Mean Collar Radius	rc	0.07
			Friction Coefficient (surfaces)	ft	0.15
			Friction Coefficient (surfaces)	fc	0.15
			tan	tan	0.0831
			secalpha	sec	1.1547

Figure 3.10. Bolt Calculator with various inputs

Bolt Stiffness			Joint		
K of shank portion	ks	#DIV/0!	Joint Constant	C	-0.1169
K of threaded portion	kt	723937	Force required to separate	Fsp	518.519
Length of shank portion	Ls	0	Factor of Safety on separation	FSsp	0.02074
Length of threaded portion within grip	Ltg	0.25			
K of entire bolt	kb	723937	Forces		
Length of Grip	Lg	0.25	Bolt tension due to preload	FbPL	579.149
			Bolt tension due to applied load	FbAL	-2923.2
			Applied Tensile Load	Fal	25000
Grip Stiffness			Total tensile force on bolt	Fbt	-2344.1
K of entire grip	Kfr	-7E+06	Applied Shear Force	Fs	25000
Bolt Stresses					
			Preload Stress	Opl	96000
			Tensile Stress	Ot	-484556
			Shear Stress	Tsh	314370
			Bending Stress	Obnd	0
			Von Mises	Ovm	1395804
			Factor of Safety	FS	2
Thread Shear					
Length of Thread Engagement	Le	0.112			
External Thread Shear Area	AtsE	0.02106			
Shear Stress in External Threads	TsE	-111309			
External Thread Factor of Safety	FSe	-0.7776			
Internal Thread Shear Area	AtsI	0.02527			
Shear Stress in Internal Threads	TsI	-92758			
Internal Thread Factor of Safety	FSI	-0.9331			

Figure 3.11. Bolt Calculator with stiffness and stress values

3.2.4 Nitrous Oxide Flow Analysis

The flow of Nitrous Oxide through hydraulic constrictions is very important to characterize 2 phased flow. Since the Nitrous Oxide is pressed to its vapor pressure (the oxidizer is self-pressurizing), any small pressure drop will result in the formation of gaseous Nitrous Oxide. Most of the computational fluid analysis is focused on the injector.

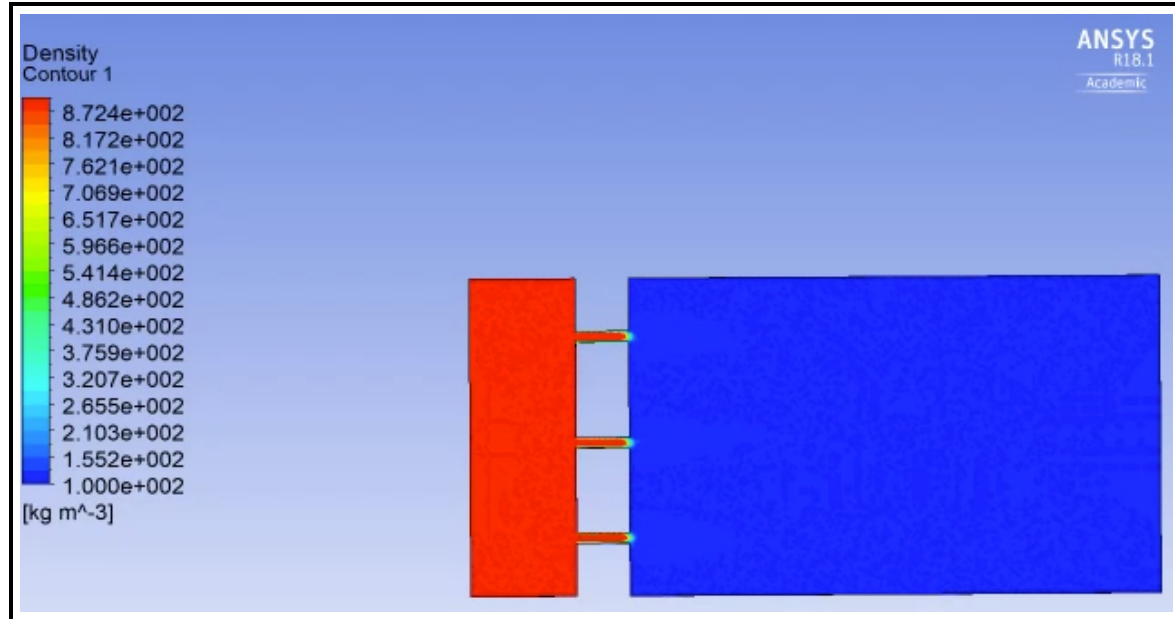


Figure 3.12. Injector Transient 2 Phase Flow at steady state

Fig. 3.12 shows the change in phase from liquid to gaseous Nitrous Oxide across orifice holes. The liquid N₂O is represented by the higher density fluid (red color) and the gaseous N₂O is represented by the lower density (blue color). The pressure drop across the orifices reduces the pressure below the vapor pressure of the incoming oxidizer causing Nitrous Oxide to flash and turn into a liquid. This snapshot of a transient 2-dimensional illustrated the effects of an injector simulation.

However, running transient simulations can prove to be computationally expensive and unnecessary. Therefore, we have been working on a simpler 2-phased model to calculate the 2-phased mass flow rate based on a pressure drop caused by an orifice. A starting point for total injection area was determined using the Non-Homogeneous Non-Equilibrium

(NHNE) two-phase mass flow rate model, otherwise known as the Dyer model [10].

$$\dot{m}_{DYER} = \left(\frac{\kappa}{\kappa+1} \dot{m}_{SPI} + \frac{1}{1+\kappa} \dot{m}_{HEM} \right) \quad (3.4)$$

The model attempts to justify the amount of vaporization that can occur inside a given injector using a non-equilibrium parameter κ , not to be confused with Nuricks cavitation number. The non-equilibrium parameter is proportional to the ratio of bubble growth time τ_b , and liquid residence time τ_r ,

$$\kappa = \sqrt{\frac{p_1 - p_2}{p_v - p_2}} \propto \frac{\tau_b}{\tau_r} \quad (3.5)$$

Depending on the value of κ , the model predicts a mass flow rate either close to the Bernoulli derived, Single Phase Incompressible (SPI) mass flow rate model,

$$\dot{m}_{SPI} = C_d A \sqrt{2\rho \Delta P} \quad (3.6)$$

or to the Homogeneous Equilibrium Model (HEM),

$$\dot{m}_{HEM} = C_d A \rho_2 \sqrt{2(h_1 - h_2)}. \quad (3.7)$$

Determining mass flow rate using the HEM model requires enthalpy both upstream and downstream of the injector, a process which becomes trivial using REFPROP 10, a NIST materials database that can be used to calculate chemical properties using highly accurate equations of state for a variety of chemicals. Using REFPROP the downstream properties can be then calculated by following a line of constant entropy between the two states, such that $S_1 = S_2$ [10].

<u>Variable</u>	<u>Value</u>	<u>Units</u>
P1 (Upstream Pressure)	2394.12698	kPa
P2 (Downstream Pressure)	2068.43	kPa
Pressure Ratio	0.863960023	Ratio
Gamma	1.31	Ratio
Temperature Ratio	0.965988106	Ratio
T2 (Downstream Temperatu	289.7964318	K
Pc (Critical Pressure)	7251	kPa
Tc (Critical Temperature)	309.57	K
T1 (Upstream Temperature)	300	K
Tr (Reduced Temp)	0.969086152	Ratio
Pv (Vapor Pressure)	5895.51862	kPa
Media	nitrous oxide	
Dynamic Viscosity Upstream	1.57933E-05	kg/ms
Dynamic Viscosity Downstre	1.52029E-05	kg/ms
d (diameter)	0.00254	m
r/d	0.001	Ratio
L/d	10	Ratio
Reh (Reynolds Number)	909500.509	Ratio
K (Nurick's Cavitation Numb	-10.7504578	Ratio
Kincep	1.895102395	Ratio
Kcrit	1.265813707	Ratio
Flow State	Flipped	
Area Upstream	9.68E-04	m ²
Area Orifice	9.68E-05	m ²
k	0.2917243	Ratio
m' (Dyer Mass Flow Rate)	3.20E-01	kg/s
Cd (Discharge Coefficient)	0.65	Ratio
rho (Density) - Upstream	49.09532817	kg/m ³
rho (Density) - Downstream	41.40955831	kg/m ³
Enthalpy - Upstream	445.5219091	KJ/kg
Enthalpy - Downstream	438.5020614	KJ/kg
m'sp	3.58E-01	kg/s
m'hem	3.09E-01	kg/s
b1	-6.71893	constant
b2	1.35966	constant
b3	-1.3779	constant
b4	-4.051	constant

Figure 3.13. 1-dimensional 2-phased flow calculator.

The 2-phased flow calculator includes an orifice sizing built in to the calculator for injector sizing and feed system validation applications. The yellow colored cells represent calculator inputs and the green cells are the outputs of the calculator (Fig. 3.13). Therefore, an upstream and downstream pressure output a 2 phase mass flow rate through an orifice. The dynamic properties of N₂O are obtained from REFPROP 10.0 and [11].

3.3 Rocket Geometry

3.3.1 Nozzle Sizing

Many of the design characteristics of the nozzle design and analysis begin with NASACEA [12]. NASACEA calculates chemical equilibrium compositions and properties of complex mixtures present during combustion within a rocket engine. This tool has been proven to be a reliable source of properties and is currently used in industry. We recommend using the python wrapped version of NASACEA called 'rocketcea' [13]. We note that NASACEA uses English Units and one must be wary of including the gravitational constant in equations to convert from lbm to lbf.

Performance is given for both Frozen and Shifting equilibrium conditions for NASACEA [14].

- Frozen equilibrium - chemical composition of the exhaust does not change as it flows through the nozzle (product composition is established in the combustion chamber).
- Shifting equilibrium - assumes that instantaneous chemical equilibrium is established as the gas expands through the nozzle, "shifting" the composition continuously.

Relevance of Both Results - because of the very short residence time in the nozzle, it is uncertain whether or not there is sufficient time for chemical reactions to actually occur as predicted by the shifting equilibrium model. Geometry also plays a role, as longer nozzles provide more residence time. Which results to use - For amateur motors, where nozzles are very small in comparison with large professional rockets, *we consider the frozen equilibrium flow model to be more realistic.*

Input Variables:

- Chamber Pressure - The pressure in the combustion chamber is a parameter that is selected through trade studies, a good initial sizing can be found by using the ratio of specific heats and the mixture ratio.
- For initial sizing, it's beneficial to begin with an initial guess and then iterate through designs until a chamber pressure can be intelligently chosen.
- Ambient Pressure - The ambient pressure that the nozzle exhaust gases will be exposed to. However, the ambient pressure changes as the rocket travels further away from the surface. Therefore, depending on where the maximum thrust is required,

the nozzle is optimized for the particular ambient atmospheric pressure. Reference Fig 3-10 in Rocket Propulsion Elements [15].

- Mass Ratio (Oxidizer to Fuel Ratio) - Depending on combustion chamber design (film cooling, thermal management, etc..), the ratio mass flow of oxidizer to mass flow of fuel is determined. The mass ratio determines the chemical properties of the combusted exhaust gases coming out of the combustion chamber and into the nozzle.
- Mass Flow Rate - This is the total mass flow rate of propellant entering the combustion chamber and nozzle.

Equation 3.8 describes the thrust generated by the momentum of the exhaust velocity of the flow and the pressure difference between the exhaust gases and ambient pressure. For this calculation, the pressure thrust goes to 0 as the nozzle is assumed to be perfectly expanded. Therefore, there is no difference between exhaust pressure and ambient pressure.

$$T = \dot{m}u_e + (P_e - P_a)A_e \quad (3.8)$$

The mass flow rate of the propellant is chosen based on the fluid system design and the requirements of the engine. Therefore, the exit velocity of the nozzle must be found to obtain the thrust.

$$\dot{m} = \frac{A_c P_t}{\sqrt{T_1}} \sqrt{\frac{\gamma}{R}} \frac{\gamma+1}{2}^{\frac{-\gamma+1}{2(\gamma-1)}} \quad (3.9)$$

Equation 3.9 [16] is the relation between propellant mass flow rate and throat area.

- Mass Flow Rate - This has been chosen based on thrust requirements.
- Total/Stagnation Pressure - The stagnation pressure of the combustion chamber is assumed to be equal to the static pressure as velocity in the combustion chamber is negligible.
- Total/Stagnation Temperature - The stagnation temperature of the combustion chamber is assumed to be equal to the static temperature as the velocity in the combustion chamber is negligible.
- Ratio of Specific Heat (Gamma) - The ratio of specific heat of the combustion gases.

The throat area is obtained by solving for A_c in Equation 3.9.

We use NASACEA Parameters (preferred as they are calculated specifically for the propellants used) to determine key thermodynamic and performance characteristics of the nozzle:

- Expansion Ratio - Depending on the propellants, NASACEA will provide the optimum expansion ratio.
- Exit Area - The required exit area of the nozzle is found by multiplying the throat area with the expansion ratio.
- Exit Gamma - Specific heat ratio of the exhaust gases at the exit of the nozzle.
- Exit Mach Number - The Mach number of the exhaust gases at the exit of the nozzle.

Next, the exhaust velocity must be calculated based on the given properties at the nozzle exit. Equation 3.10 [2] is used. The exit velocity is an important parameter as it contributes significantly to thrust. This equation assumes that gas velocity in the combustion chamber is negligible. This is a reasonable assumption to make for ideal nozzle analysis.

$$v_e = \sqrt{\frac{2g\gamma}{\gamma-1} RT_c \left(1 - \frac{P_e^{\frac{\gamma-1}{\gamma}}}{P_c}\right)} \quad (3.10)$$

Equation 3.10 gives the relation between exit velocity and the pressure ratio from the nozzle inlet to nozzle exit:

- g - Since this equation is specifically given for English units, the gravity constant is included in this equation.
- Ratio of Specific Heat (Gamma) - The ratio of specific heat of the combustion gases.
- Exit Pressure (Pe) - Pressure at the exit of the nozzle.
- Total/Stagnation Pressure (Pc) - The stagnation pressure of the combustion chamber is assumed to be equal to the static pressure as velocity in the combustion chamber is negligible.
- Total/Stagnation Temperature (Tc) - The stagnation temperature of the combustion chamber is assumed to be equal to the static temperature as the velocity in the combustion chamber is negligible.

Exhaust velocity of the gases is obtained. Now, we can go back the Equation 3.8 and substitute the values of mass flow rate, pressure differential, exit area, and exhaust velocity to obtain thrust.

3.3.2 Determining Nozzle Geometry

Bell Nozzles and Conical Nozzles can be used for most applications. Bell nozzles are preferred over conical nozzles as they are shorter in length, but still provide the same expansion ratio (smaller length ensures lower overall mass). However, we begin with a conical nozzle approximation.

Since the inlet area and exit area are known (and hence the radii), assume a 15° divergent half angle. *This is rule of thumb suggested in [2]

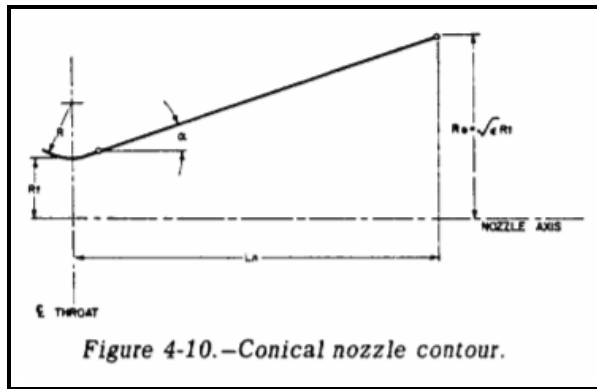


Figure 3.14. Dimensions of Sizing a Conical Nozzle [2]

Use Equation 3.11 [2] given below to determine nozzle length.

$$L_n = \frac{R_t(\sqrt{\epsilon} - 1) + R(\sec \alpha - 1)}{\tan \alpha} \quad (3.11)$$

- R_t - Throat Radius
- R - According to Fig 4.3, R is 1.5 times R_t .
- ϵ - Expansion ratio from NASACEA code.
- α - Nozzle half angle.

The length of an ideal bell nozzle is equivalent to 80% of the length of an ideal conical nozzle while giving similar performance [2].

The Bell nozzle entry and exit angles are the end constraints that can be given for a Bezier Curve. Based on the area ratio, a combination of inlet and exit angles can be

selected:

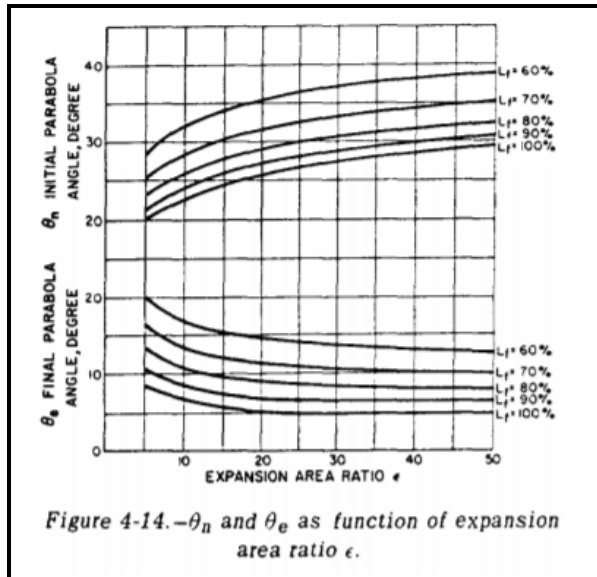


Figure 3.15. Nozzle Entry and Exit angles based on expansion ratio [2]

The most common Bezier profile used is the G.V.R. Rao parabolic approximation. Although this profile may not be the most optimal for all applications, following this approximation will ensure generalized and simplified approach to Bell Nozzle design.

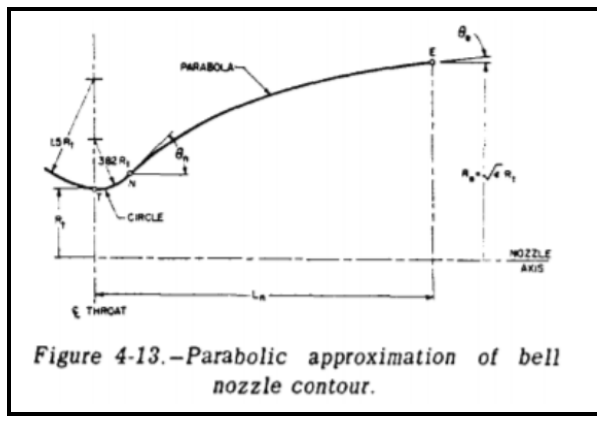


Figure 3.16. Dimensions of Sizing a Nozzle [2]

Preliminary nozzle sizing is complete - these results must be validated and refined using CFD or Method of Characteristics.

Performance Parameters and Validation

How to determine the design quality:

- I_{sp} - This parameter is specific impulse. The meaning of specific impulse is the amount of thrust produced per unit mass flow rate (similar to mileage of a car). Based on the given propellants and nozzle sizing, a higher the specific impulse connotes a more efficient design. The SpaceX Merlin engine has an I_{sp} of 282s and the Saturn V F-1 engines have an I_{sp} of 263s.
- C^* - Characteristic velocity is a measure of combustion performance. This quantity determines the propellant mass flow rate required to maintain the required nozzle stagnation pressure. This parameter is dependent on propellant chemistry and design of injector/combustion chamber.

How to validate calculations:

- Work with team member in parallel to fact check the calculations and debug code to ensure the correct parameters are used in each equation.
- Reference the specifications of engines like the F-1, Merlin, and RS-25. Try to run the code with the input parameters of these engines and try to match the output.
- Reference the A-1 [2] engine calculations to follow the various equations and methodology.
- Expect the calculations to be a little different and this is an ideal nozzle calculator and actual nozzle performance is affected by losses not reflected in the code.

Results of applying these calculations to the Taurus II designs are shown in App. F.

3.3.3 Combustion Chamber Sizing

The other significant contributor to engine performance is the design of the combustion chamber. Essentially, the chamber must be sized properly to accommodate the incoming combustion gases and ensure a low upstream gas velocity. This low velocity is desired to ensure all energy is converted to thermal energy. We begin by exploring at some correlations and empirical parameters for combustion chamber sizing.

3.3.4 Combustion Chamber Length

Characteristic Length (L_*) is a normalized value of combustion chamber length required for the complete combustion of specific propellants. Reference the table below for these empirically determined values.

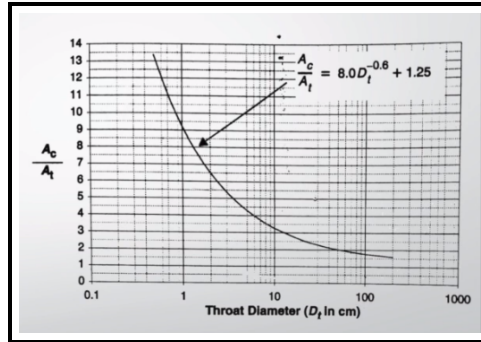


Figure 3.17. Correlation of Combustion Area to Throat Area [3]

The chamber area given by Figure 3.17 can be validated using Table 3.4 [15]. According to this table, pressure losses in the chamber can be neglected if the Chamber-to-Throat Area Ratio is greater than 3.5. Finally, the length (L_c) of the combustion

Table 3.4. Estimated Losses for Small-Diameter Chambers [15]

Chamber-to-Throat Area Ratio	Throat Pressure (%)	Thrust Reduction (%)	Specific Impulse Reduction (%)
∞	100	0	0
3.5	99	1.5	0.31
2.0	96	5.0	0.55
1.0	81	19.5	1.34

chamber can be determined using Fig. 3.18.

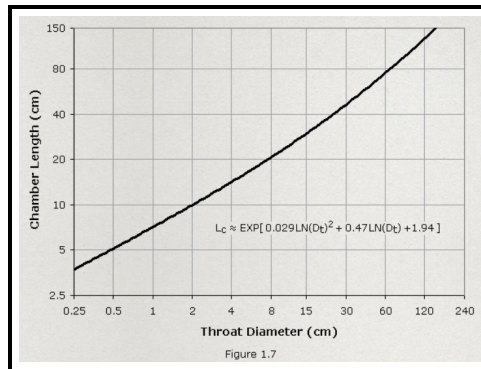


Figure 3.18. Correlation of Chamber Length to Throat Diameter [4]

Reference Fig. 3.19 for dimensions.

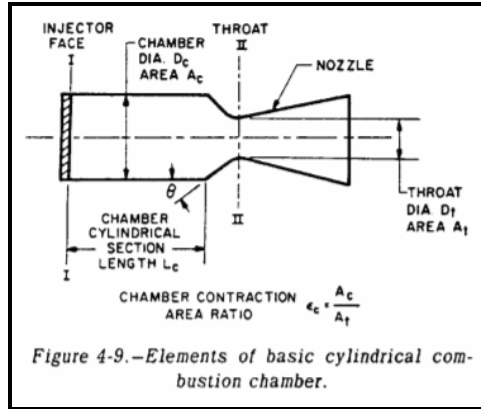


Figure 3.19. Dimensions of the combustion chamber [2]

Combustion Chamber Volume and Area

The following correlations are useful for initial sizing of the combustion chamber. However, these dimensions must be validated using CFD or experimental testing to properly characterize the engine. Combustion Chamber Volume is given by Equation 3.12 [2]

$$V_c = A_t (L_c \epsilon_c + \frac{1}{3} \sqrt{A_t} \pi \cot \theta (\epsilon_c^{1/3} - 1)) \quad (3.12)$$

- V_c - Combustion Chamber Volume
- A_t - Throat Area
- ϵ_c - Chamber Contraction Ratio
- θ - Chamber Convergent Angle (Usually between 20° to 45° - [2])

Combustion Chamber Surface Area is given by Equation 3.13 [2]

$$A_c = 2L_c \sqrt{\pi \epsilon_c A_t} + \csc \theta (\epsilon_c) \quad (3.13)$$

- A_c - Combustion Chamber Area
- A_t - Throat Area
- ϵ_c - Chamber Contraction Ratio

- Theta - Chamber Convergent Angle (Usually between 20° to 45° [2])

The methodology explained above provides some basic analysis that can be performed to size a combustion chamber. Results of applying these calculations to the Taurus II designs are shown in Appendix F.

3.4 Thermal Analysis

One of the most important considerations for rocket engines is thermal management and the characterization of the thermal stresses as a result. Figure 13 shows the application of a steady state thermal capacitance model[17]. We have taken this steady state application and discretized the heat flow increments in accordance to total burn time of four seconds.

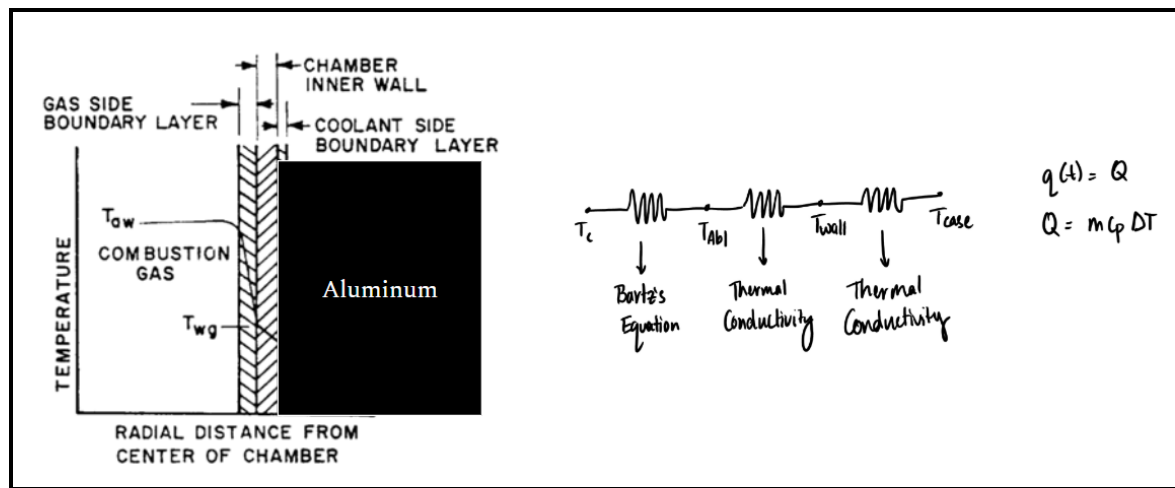


Figure 3.20. 1-dimensional thermal model [2]

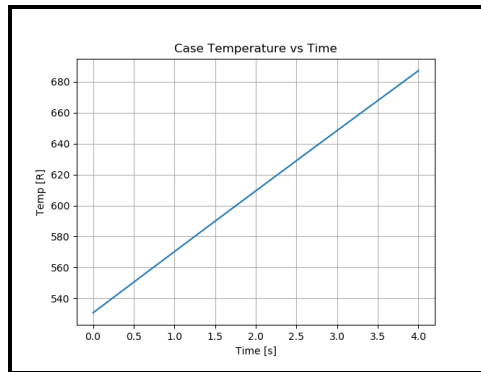


Figure 3.21. Case temperature increase over time

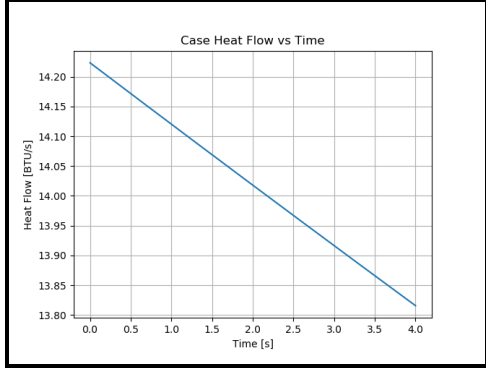


Figure 3.22. Heat flow into case over total operating time

Fig. 3.21 shows the results of the thermal analysis and the increase of the external case temperature over the total engine operation time. The results indicate a 320-degree Fahrenheit increase. Fig. 3.22 validates and provides insight into the 3-dimensional heat transfer into the case. The simulation indicates a 312-degree Fahrenheit increase in temperature shown in Appendix D.12. A graphical representation of the temperature distribution of the casing over time is shown in Appendix D.6 to D.10. Therefore, the simplified heat-sink model can be quite accurate and use as a reasonable approximation with a safety factor.

In addition to this 1D simulation, the heat flow values obtained from Fig. 3.22 were used as the input values for the 3D ANSYS validation simulations, the results of which are shown in Appendix D. Dr. Bogard recommended that we validate the 2D heat transfer model with an FEA analysis [7]. ANSYS 19 allows the load coupling between thermal and structural simulations. The thermally coupled load results in a diminished safety factor for the case. We have optimized the case thickness the thermal protective material to ensure the minimum safety factor is met. Since LRA has already bought the Aluminum stock the machine the engine, the ablative and ceramic thickness become the driving optimization factor for this rocket engine. The results from the transient thermal analysis, Fig. D.3 and Appendix D.11 were imported into a transient structural analysis solver to combine the pressure stress and thermal stress exerted on the case. The fixed supports (purple) are shown to be the bolt holes as this section will be attached to the rocket airframe. The pressure and

thermal loading are applied to the inner surface of the engine case. This structural analysis will allow for determination of the minimum safety factor.

The results shown in Fig. D.3 display the range of minimum safety factors for the casing. The lowest safety factor is 1.34. This result can be ignored as the 1.34 safety factor is near the bolt holes. In reality, the bolt holes will be supported by the retaining rings and are significantly above the safety factor shown by the FEA analysis. The area of interest is the high temperature combustion chamber case area. Near the areas with the maximum deflection, the minimum safety factor of 2.5. This exceeds the minimum safety factor requirement of 2. Therefore, even though the Aluminum casing becomes quite hot, the structural integrity is maintained.

From the stress analysis results, Fig. D.5 shows the deflection of the case under thermal and structural load. The deflection at the end of the casing is extremely small so residual stresses will not be a large factor. Furthermore, the maximum deflection is concentrated at the combustion chamber. When integrating the engine in the rocket, sufficient gap should be given between the airframe and engine casing for thermal and structural considerations.

3.5 Thermal Model Calculations

The design of the regenerative cooling system began with an analysis of convective heat transfer from the hot combustion gases to the gas-side chamber wall.

Temperatures referenced in Figure 3.20:

- T_{aw} - Bulk Combustion Temperature (R)
- T_{wg} - Wall Temperature (R)

$$Pr = \frac{4\gamma}{9\gamma - 5} \quad (3.14)$$

Equation for Prandtl Number [2]

$$\mu = (46.6 \times 10^{-10}) M^{0.5} T^{0.6} \quad (3.15)$$

Equation for Viscosity [2]

Combustion chamber Prandtl number is calculated based on the specific heat ratio (γ) in various sections of the engine. Through NASACEA, the specific heat ratio in the combustion chamber, throat and nozzle can be obtained. The viscosity is calculated based on regional temperature (T) and local molecular weight (M). NASACEA provides this information in the combustion chamber, throat and nozzle. So, the updated Prandtl number and viscosity with varying engine combustion parameters are calculated.

$$\sigma = \frac{1}{\left[\frac{1}{2} \frac{T_w g}{T_c} \left(1 + \frac{\gamma-1}{2} M^2 \right) + \frac{1}{2} \right]^{0.68} \left[1 + \frac{\gamma-1}{2} M^2 \right]^{0.12}} \quad (3.16)$$

Sigma Parameter required for Bartz's Equation [2]

Sigma relates the engine temperatures (T_{wg} , T_c) and chamber local Mach number (M). This relation allows the calculation of the heat transfer coefficient over a range of allowable wall temperatures (if the engine wall is fabricated with ceramic inserts at the nozzle) and the Mach number variation influencing convective heat flux.

$$h_g = \left[\frac{0.026}{D_t^{0.2}} \left(\frac{\mu^{0.2} C_p}{Pr^{0.6}} \right) \left(\frac{P_c g}{c^*} \right)^{0.8} \left(\frac{D_t}{R} \right)^{0.1} \right] \left(\frac{A_t}{A} \right)^{0.9} \sigma \quad (3.17)$$

Bartz's Equation [2]

The heat transfer coefficient (h_c) is found using Bartz's equation correlation. The heat

transfer coefficient is a function of local engine cross-sectional area. Therefore, the heat transfer coefficient at various points in the engine can be determined given a engine geometry spline (function of engine radius versus length).

$$H = \frac{1}{\frac{1}{h_{Bartz}} + \frac{t}{k_{cer}} + \frac{t}{k_{abl}}} \quad (3.18)$$

Thermal Resistances [2]

The thermal resistance for resistive layers can be calculated using thermal conductivity (k) and the applicable thickness (t). It is known that RP-1 and liquid oxygen combustion produces a soot layer that aids with thermal protection of the chamber walls. However, a reliable prediction of the thickness of this layer based on the oxidizer-to-fuel ratio and burn time has yet to be obtained. Therefore, this consideration will be omitted from the analysis until test data is obtained to predict this value. To aid with coolant temperature minimization, a Zirconia based ceramic liner ($t = 0.002$ in) has been incorporated in the thermal resistance analysis. Preliminary research shows that such ceramics have been used successfully used in previous rocket engines and can withstand the fluid forces during operation.

$$dT_c = \frac{Q}{\rho V \lambda} dt \quad (3.19)$$

Specific Heat Equation [17]

The heat flow (Q) into the casing causes a temperature rise. The rate at which the temperature increases is driven by the specific heat () of the case (heat sink). This equation is used in an iterative loop that determine temperature change per time step.

$$Q = HA(T_{inf} - T_{case}) \quad (3.20)$$

Specific Heat Equation [17]

The incremental change in case temperature affects the heat flow. Therefore, the heat flow is calculated with the updated case temperature (T_{case}). The combustion chamber temperature (T_{inf}) is assumed to be constant through out the burn. This is an assumption and the fidelity of the model if the combustion temperature over time can be found.

3.6 Thermal Protective Materials Study

The combustion temperature of rocket engines is often far higher than the melting point of the combustion chamber. In Taurus II, for example, depending on the oxidizer/fuel (O/F) ratio, the nitrous oxide and HTPB will burn at up to approximately 3100C, but the aluminum chamber around it will melt at a relatively low 600C. In order to protect rocket materials, therefore, rocket designers have developed a number of solutions.

These cooling methods can generally be classified into three groups: liquid cooling, film cooling, and ablatives. Liquid cooling systems run heat absorbing liquid (often the rocket fuel itself before combustion) through channels in the body of the rocket, while film cooling systems create a thin layer of vapor (again, usually fuel) on the chamber wall via fine orifices. Both these systems, due to their nature, can usually only be implemented in liquid rocket engines. For Taurus II, therefore, we must use an ablative system: materials lining the interior of the combustion chamber for thermal protection. Most of these materials redirect heat by combustion and melting away (hence "ablative"); still, a very few materials do not ablate, so we shall generally refer to the general category of material linings as "thermal protective materials", which can be ablative or non-ablative.

Ablative materials are designed for low thermal conductivity, high heat capacity, combustion under chamber conditions, and some amount of abrasion resistance (in addition to

low density, of course). Combustion gases will heat the material to its melting or combustion point, at which point it will liquify or incinerate and leave the engine, with absorbed heat, through the nozzle. At the same time, the material must resist abrasion by material in the combustion chamber so that it is not carried away by mechanical force, which does not contribute to heat reduction. Most ablatives are a composite material of combustible organic resin in some inorganic matrix (see Table 3.5). Ablatives can be very effective, but must be replaced after use. For this reason, they are very common in solid and hybrid rocket engines, in which the fuel, too, must be replaced, but less widely used in liquid fuel engines.

Table 3.5. Assorted matrix and filler materials for ablative composites.

Matrix	Filler
epoxy	fiberglass
silicone	woven carbon, nylon, or quartz
temperature resistant phenolic	asbestos

Non-ablatives are protective films able to withstand the combustion temperature directly. These are usually produced using ceramics or metals (e.g., tungsten, which, while extremely heavy, melts at 3420C). Non-ablatives must be designed for low thermal conductivity, high heat capacity, and abrasion resistance like ablatives, but are not expected to combust. Low density is also important, of course, for weight savings (ruling out tungsten). These are much more difficult to build, but are reusable. The space shuttle heat shield, mostly reinforced carbon-carbon (RCC), is a non-ablative thermal protective material (notably, the explosion space shuttle Columbia resulted from an impact that broke through the RCC panels of the shuttle, allowing gases to enter a wing).

Taurus II requires some sort of thermal protective material. Ablative materials tend to be cheap and common compared to non-ablatives, so ablatives are common among other amateur rocketry teams. In particular, fiberglass, which is normally used as a lightweight airframe material, happens to have good ablative properties (see Table 3.6): it is quite

feasible to layer the inside of the engine with fiberglass to sufficient thickness to protect the chamber walls.

Table 3.6. Important material properties of typical fiberglass. The glass transition temperature is used instead of melting point as the matrix resin combusts at some higher temperature. The exact properties vary widely between resin and glass fiber formulations.

Material	Fiberglass (typical)
Thermal Conductivity (W/m-K)	1.2
Specific Heat (J/kg-K)	800
Glass Transition Temperature (°C)	> 100
Density (kg/m ³)	2600

Non-ablatives are much more difficult to find. Because we do not have access to advanced materials fabrication facilities, LRA is limited to commercial off-the-shelf coatings. While no company sells material marketed as a non-ablative thermal protective material, refractory (high-temperature) coatings are commonly used in forges and jet engines. Even in this industry, however, the Taurus II 1800C temperature is high—a materials engineer for an aluminum foundry company (Pyrotek) did not know of any such materials. Another company, ZYP Coatings, offered more alternatives. Apparently, multiple oxides are often used as coatings, with zirconium oxide being chief among them. ZYP offers easily applicable (aerosol and liquid paint) coatings of zirconium oxide, ytterbium oxide, boron nitride, and other materials, but only a particular zirconium oxide variant may have the material properties to withstand the rocket engine. This oxide must be stabilized by another material, say, calcium, to prevent a crystal structure change that can lead to cracking when cooling, but can withstand our temperatures. Finally, coatings should be applied in thin layers (2-4 micron), again to prevent cracking. More complete bulk material properties are listed in Table 3.7. We note, however, that the exact properties of these films are near impossible to measure with current technology and may only approximate the bulk. For example, ZYP claims its zirconium oxide coating becomes slightly porous upon solidifying, which may negatively affect its abrasion resistance properties.

For Taurus II, use of non-ablative materials may prevent molten ablative from affecting

Table 3.7. Important material properties of bulk calcium-stabilized zirconium oxide. Thin films may differ due to microstructure changes. Note that all properties are worse than fiberglass in exchange for a much higher melting point.

Material	Zirconium Oxide
Thermal Conductivity (W/m-K)	1.6
Specific Heat (J/kg-K)	630
Melting Point (°C)	2700
Density (kg/m ³)	5000

the reusability of the nozzle (experience shows that molten material is hard to remove from graphite, which the nozzle is machined from). However, as only thin films may be applied, we recommend LRA combine multiple materials. In particular, coating a fiberglass ablative with zirconium oxide may act as a single non-ablative material of any desired thickness, with exact dimensions to be determined by the thermal analysis outlined in this report. We do note the glass transition temperature of fiberglass is low, so this combination may react in difficult-to-predict ways to combustion. We suggest experimental trials. Also, a layer of non-ablative material between the fiberglass ablative and outer aluminum engine casing may allow the fiberglass to be replaced easily.

3.7 Financial Overview

A brief overview of the budget and expenses will be discussed to help provide a more holistic view of the design project. A quick list of associated costs is listed in Table 3.8 below. The stock material for the engine housing includes Aluminum 6061 because its cost-effective, lightweight, and easily machinable compared to the heavier and expensive Stainless-Steel counterparts. The engine casing, post-combustion chamber, and injector manifold will also be constructed using Aluminum 6061. The Isomolded Graphite Nozzle is expensive but necessary because its less prone to erosion and has high service temperatures. The entire manufacturing apparatus and HTPB fuel grain costs \$132.63. The manufacturing setup is optimized to minimize pockets of air within the fuel grain and allows for a maximum thrust. The ablative liner to be used (Zirconium Oxide) costs about

\$160 per quart and will have to be cleaned and replaced with each hotfire. As of now, the fuel grain and the ablatives are the only components that have to be replaced with each test. For the hardware and fasteners, its an estimated \$196.78 for the engine retention, injector plate, high-temperature silicone ORings, and connections. This brings the total estimated cost for the project to around \$927.57. The temperature resistant ablative liner allows us to use aluminum as the engine body instead of steel and saves a large portion of costs and manufacturing obstacles. It would limit the frequency of hotfire tests and prevent accurate and timely results.

Table 3.8. Project budget estimates

Item	Cost (\$)
Extruded Bare Tube T6	47.30
Extruded Bare Tube T6	32.88
Extruded Round T6511	119.20
Isomolded Graphite Rod	238.78
Fuel Grain Manufacturing Assembly	62.64
HTPB (per gallon)	69.99
Ablative Liner (per quart)	160.00
Engine Retention Bolts	54.70
Injector Plate Bolts	15.90
ORings	58.40
Connection Bolts	67.79
<i>Total Cost</i>	927.5

3.8 Test Site Details

The hotfire tests of Taurus I/II will be conducted at a remote facility using the Longhorn Rocketry Association infrastructure. The facility location at Pickle Research Center consists of an aluminum shed which houses the mounted engine and is located in front a concrete wall/blast shield to absorb the impact of the thrust. The Fluid Panel is already built and maintained by LRA. About 100 feet from the engine test stand is a remote building that houses the DAQ System, remote trigger, and controls system where all operations and measurements can be controlled remotely to ensure safe tests as per proper protocol required by UT.

During the course of this project, a second Cold Flow test has been performed to further refine test site procedures. A Cold Flow consists of all steps followed for a hot fire test without the ignition event. This exercise allows for practice and perfection of test site operations. A successful Cold Flow was concluded on 04/27/2019. Dr. Leon Vanstone, test site supervisor for LRA, has given the team permission to pursue a hotfire within the coming weeks. The team is furiously working on the final additions to the test stand in preparation of a Taurus I engine test. This is a huge milestone for LRA and our team.

4 CONCLUSIONS AND RECOMMENDATIONS

The scope of this project is to design and analyze the Taurus II flight-weight rocket engine and provide assistance for the Taurus I test bed engine hotfire. We were able to optimize a significant portion of this engine and perform a successful Cold Flow.

The fuel grain is cast into a suitable mold, but often contains up to 10% volume of air bubbles, which make the engine thrust nonuniform and reduce energy density. By casting the fuel in a vacuum chamber, we were able to remove all visible bubbles from the grain. Furthermore, we programmed a fuel grain regression rate simulator that can determine how this surface area changes over time. Using this to optimize the fuel grain channel shape, we found geometries that can reduce thrust uniformity by up to 7x or, at the cost of uniformity, provide up to (an optimistic) 50% more thrust, which can also be traded for a 3.4lb weight savings, 7% of the total engine weight. These numbers should be empirically verified.

Next, we simulated the structure of the engine under expected thermal and mechanical loading. We found LRA's proposed engine casing satisfied the safety factor of 2 required by the SAC with a slightly thinner ablative (heat protection) inner layer. We also verified the strength of the bolts used to assemble the engine.

Finally, we analyzed the fluid flow through the engine. CFD determined the injector nozzles will successfully vaporize all N₂O, and we optimized the nozzle and combustion chamber sizes. Most importantly, changing the oxidizer-to-fuel ratio gives about 16% more thrust.

All these results will now be given to LRA. In addition, simplified calculators—the fuel grain regression simulator, a 1D heat transfer network, a bolt strength calculator, and nozzle and combustion chamber calculators—were developed so that LRA can further optimize Taurus II or future engines if they choose. We believe these results, which, if all implemented and tested, may increase empirical thrust by over 50%, are significant, and, if nothing else, LRA has more confidence in its engine design and can begin manufacture to test the Taurus II hybrid engine before the summer 2020 SAC competition.

REFERENCES

- [1] H. O. Toft, “Voids in solid propellants.” [Online]. Available: http://dark.dk/documents/technical_notes/voids.pdf
- [2] D. K. Huzel and D. H. Huang, *Design of Liquid Propellant Rocket Engines*. National Aeronautics and Space Administration.
- [3] U. L. P. Laboratory, “Lccls - rocket engine sizing.”
- [4] R. Braeunig, “Basics of space flight: Orbital mechanics.” [Online]. Available: www.braeunig.us/space/propuls.htm
- [5] A. Bath, “Performance characterization of complex fuel port geometries for hybrid rocket fuel grains,” Master’s thesis, Utah State University, Logan, Utah, 2012.
- [6] O. Krauss, “Design and test of a lab-scale n₂o-htpb hybrid rocket,” 2003.
- [7] “Fluent documentation 16.2.” [Online]. Available: www.sharcnet.ca/Software/Ansys/16.2.3/en-us/help/ai_sinfo/flu_intro.html
- [8] F. W. Team, “Screw thread design.” [Online]. Available: <https://www.fastenal.com/en/78/screw-thread-design>
- [9] “Bolted joint analysis.” [Online]. Available: <https://mechanicalc.com/reference/bolted-joint-analysis>
- [10] B. J. Soloman, “Engineering model to calculate mass flow rate of a two-phase saturated fluid through an injector orifice,” 2011.
- [11] “Thermophysical properties of nitrous oxide.”
- [12] NASA, “Nasa chemical equilibrium with applications.” [Online]. Available: www.grc.nasa.gov/www/CEAWeb/
- [13] “Rocketcea wraps the nasa fortran cea code and provides some useful tools.”
- [14] R. Nakka, “Solid rocket motor theory – guipep.” [Online]. Available: www.nakka-rocketry.net/th_prope.html
- [15] G. P. Sutton and O. Biblarz, *Rocket Propulsion Elements, 9th edition.* Wiley.
- [16] NASA, “Rocket thrust summary.” [Online]. Available: www.grc.nasa.gov/www/k-12/airplane/rktthsum.html
- [17] . L. A. Bergman, T. L., *Fundamentals of Heat and Mass Transfer*. Hoboken, NJ: John Wiley Sons, 2017.

APPENDIX A: Gantt Chart

The team developed a Gantt chart, reproduced in Fig. A.1 and Table A.2 to plan and ensure said plans could proceed in time for completion by the end of the semester project due date.

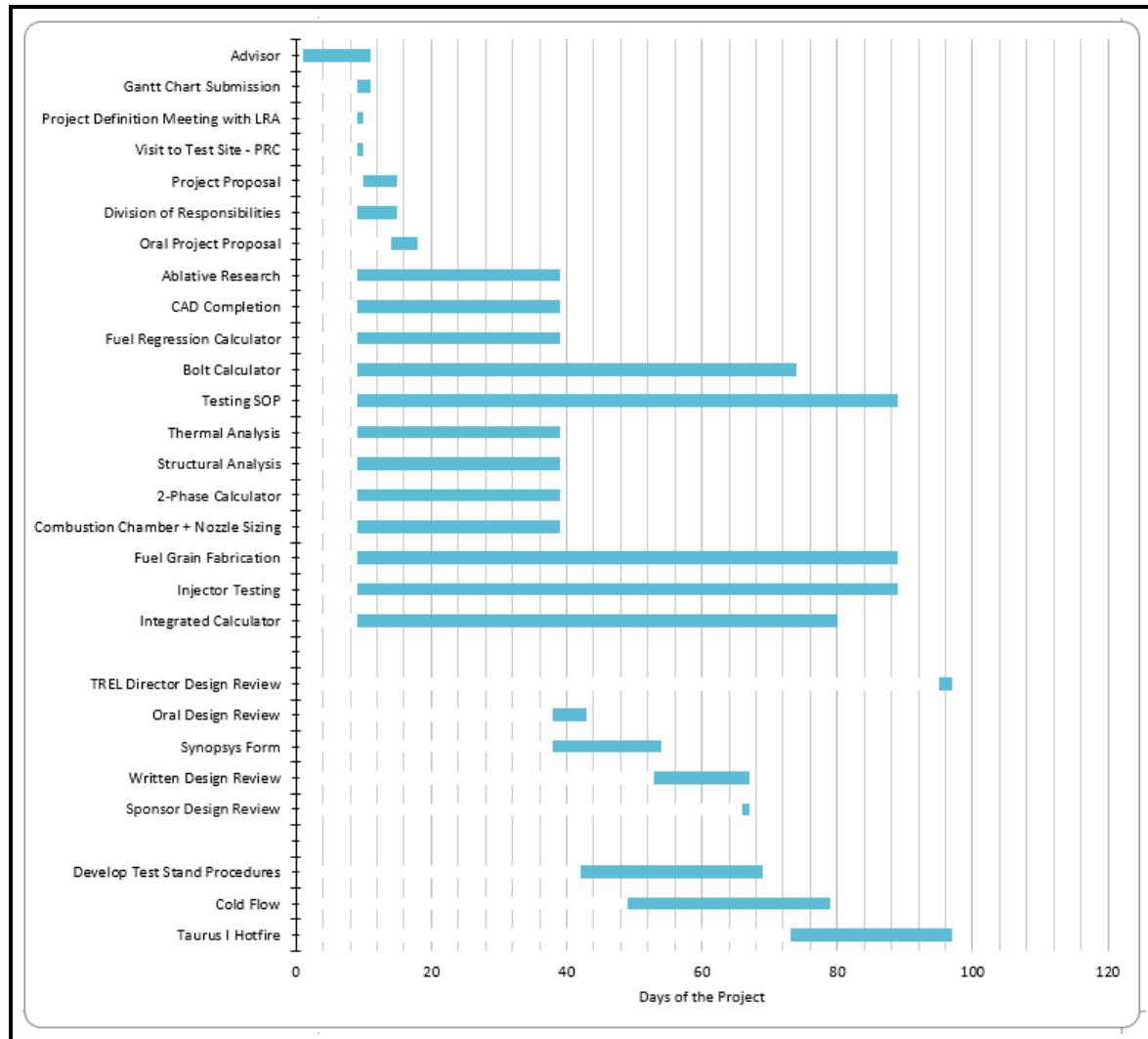


Figure A.1. The current project schedule, as a Gantt chart

Task Name	Start Date	End Date	Start On Day*	Duration* (Work Days)	Team Member	Percent Complete
Hybrid Rocket Engine Research						
Advisor	2/1	2/10	1	10	Team	100%
Gantt Chart Submission	2/10	2/11	9	2	Team	100%
Project Definition Meeting with LRA	2/10	2/10	9	1	Team	100%
Visit to Test Site - PRC	2/10	2/10	9	1	Team	100%
Project Proposal	2/11	2/15	10	5	Team	100%
Division of Responsibilities	2/10	2/15	9	6	Team	100%
Oral Project Proposal	2/15	2/18	14	4	Team	100%
Ablative Research	2/10	3/11	9	30	Daniel	100%
CAD Completion	2/10	3/11	9	30	Daniel	100%
Fuel Regression Calculator	2/10	3/11	9	30	Daniel	100%
Bolt Calculator	2/10	4/15	9	65	Shane	100%
Testing SOP	2/10	4/30	9	80	Akshay	100%
Thermal Analysis	2/10	3/11	9	30	Akshay	100%
Structural Analysis	2/10	3/11	9	30	Akshay	100%
2-Phase Calculator	2/10	3/11	9	30	Akshay	100%
Combustion Chamber + Nozzle Sizing	2/10	3/11	9	30	Akshay	100%
Fuel Grain Fabrication	2/10	4/30	9	80	Mahdi	100%
Injector Testing	2/10	4/30	9	80	Mahdi	0%
Integrated Calculator	2/10	4/21	9	71	Daniel	0%
Design Review						
TREL Director Design Review	5/7	5/8	95	2	Team	0%
Oral Design Review	3/11	3/15	38	5	Team	100%
Synopsis Form	3/11	3/26	38	16	Team	100%
Written Design Review	3/26	4/8	53	14	Team	100%
Sponsor Design Review	4/8	4/8	66	1	Team	100%
Testing (Tentative)						
Develop Test Stand Procedures	3/15	4/10	42	27	Shane	100%
Cold Flow	3/22	4/20	49	30	Shane	100%
Taurus I Hotfire	4/15	5/8	73	24	Akshay	0%
Final Report						
Final Oral Presentation	4/22	4/26	80	5	Team	0%
Final Report	5/6	5/7	94	2	Team	0%

Table A.1. This current project schedule, as a table

Due to weather constraints and team availability, we have not been able to meet the Taurus I hot fire goal for this semester. This was a stretch goal. However, work for conducting a hot fire test continues and this will be an amazing accomplishment for the end of this semester. We did not have time to test injectors due to lack of time and resources during the course of this project. Since we removed the manufacturing of the Taurus II from the project scope, we did not schedule a design review with the director of Texas Rocket Engineering Labs (TREL), which would have been necessary to do so.

In return, we have added the creation of calculators for various engine components to be used and improved by LRA members for future engine designs that will be handed off to LRA. LRA members have begun the fabrication of Taurus II with our recommendations.

APPENDIX B: Patent Search

While rocket engine research is most often published as an article in a scholarly journal, the US patent repository is another potential source of prior art. We conducted a patent search here order to find inventions that might inform our optimization and design choices during this project. In particular, we are interested in previous work on thermal protective materials and fuel grain manufacturing. We divided our patent search, conducted via the USPTO website search tool [CITE] and Google Patents [CITE], into these two areas.

B.1 Fuel Grain

Patent 9,822,045, "Additive Manufactured Thermoplastic-Aluminum Nanocomposite Hybrid Rocket Fuel Grain and Method of Manufacturing Same", describes the 3D-printing of a fuel grain. In particular, a fuel mixture is extruded into a hollow cylinder—the traditional fuel grain geometry—and computer control forms waves in each layer such that the final cylinder has very narrow channels running through its cross section (see Fig. B.1). Furthermore, the preferred embodiment uses ABS as its base material. In particular, the UT engineering makerspace has 3D printers that can easily create these fuel grains. This is a potentially simpler alternative to our casting process. However, we estimate each fuel grain would take at least one week to print, which makes this method impractical at the moment. This is a continuation of patent 9,453,479 ("Solid fuel grain for a hybrid propulsion system o a rocket and method for manufacturing same").

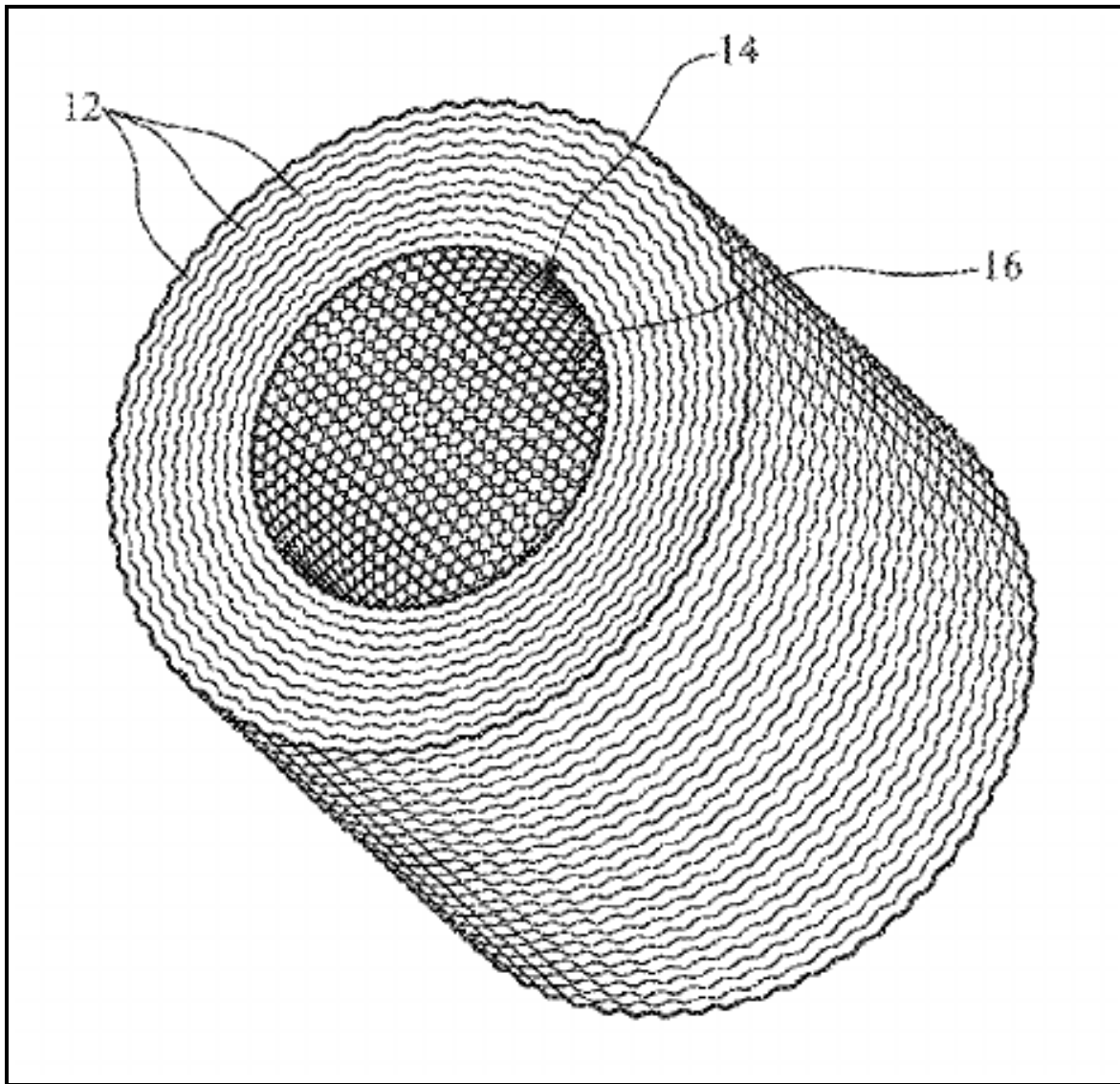


Figure B.1. An additively manufactured fuel grain. Fuel is laid down in paths (12) as is typical for FDM printing processes, and ripples in these paths (14) form channels through the grain (16) for faster combustion.

Patent 9,086,033, "Additive manufactured propulsion system", attempts to additively manufacture not only the fuel grain but the entire combustion chamber. These are proposed for cubesats, popular small (10cm) satellites that are standardized and cheap to launch, but too tiny to easily contain conventional propulsion systems. The patent suggests using any of several polymers including HTPB, ABS, PVC, and PMMA. As previously stated, 3D printing any significant portion of our fuel would take inconvenient amounts of time, so

this patent is not immediately useful. However, it is useful to know such common plastics are also good fuel candidates. Yet another patent, 8,844,133, "Stereolithographic rocket motor manufacturing method", also claims additive manufacturing of the fuel grain, to which we react the same way.

Since LRA already owns most materials for casting HTPB fuel grains, we narrowed our search to methods of better forming the grain. Since additive manufacturing is too slow, we turned to traditional casting methods. Unfortunately, the USPTO patent search was not able to find patents fitting such broad constraints. Instead, we turned to Google Patents search, upon which we found patent 5,594,177, "Shaker Table", which merely details the construction of a shaker table, which is well-known in the resin-casting community [CITE].

B.2 Thermal Protective Material

Patent 3,210,233, "Heat insulating and ablative structure and method of making same", describes a method of making an ablative protective material for spaceship atmospheric reentry protection, although the same material could, say, line a blast furnace. The ablative is a metastructure formed of a fiberglass honeycomb filled with some other material, of which many examples, organic and inorganic both, are given (see Fig. B.2). The filler may be chosen for superior thermal properties, e.g., a low thermal conductivity, high specific heat, and formation of a thick boundary layer upon ablation to reduce heat flux, while the honeycomb adds structural strength. This patent is informative because it describes many suitable materials that can be further researched—for example, alternatives to the standard fiberglass in the honeycomb include woven quartz, asbestos, and graphite, and the resin could be temperature resistant phenolic, epoxy, or silicone. Unfortunately, LRA has rather limited material processing abilities, so a honeycomb mesh is not feasible, but if a fiberglass material is used as the ablative, it is useful to know what sorts of high-temperature resins are available. In addition, one filler inorganic material mentioned is zirconium oxide, which we discovered previously in searches for high-temperature refractory coatings. This patent confirms such a material choice may be valid.

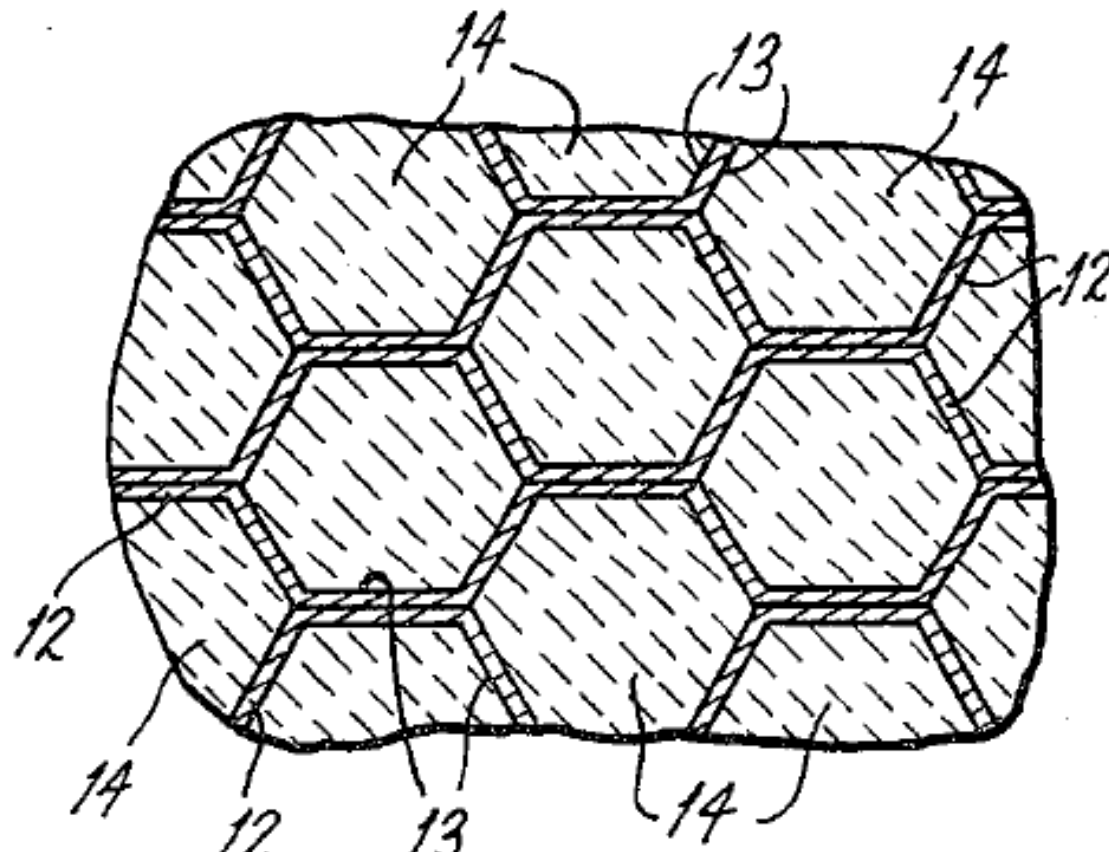


FIG. 4.

Figure B.2. An ablative material consisting of a hexagonal truss reinforcement (12), of fiberglass or similar (nonmetallic) material, and an ablative material (14) filling the interior of the hexes (13) of the truss.

Patent, 3,428,464, "Refractory coating compositions", describes a chemical method used to keep colloidal silica powders in a solution to easily paint onto a surface to form a high-temperature refractory coating; apparently, previous paints tended to separate easily. Since the patent was issued in 1969, however, we expect paintable ceramics to have become a solved problem.

Interestingly, zirconium oxide is not only a high-temperature refractory coating but a biosafe, low friction, highly wear resistant coating for prosthesis (patent 5,180,394, "Zirconium oxide and nitride coated prosthesis for wear and corrosion resistance").

APPENDIX C: Fuel Grain Test Procedures

C.0.1 Fuel Grain Fabrication Test Plan–Control

Calculations:

- Liquid HTPB to Binding compound (Papi 94 - polymethylene polyphenylisocyanate)
= 86 to 14
- Fuel Grain Curing Time = 24 to 48 hours

Supplies:

- Mixing Cups (4)
- Wooden mixing stick
- Scale
- Liquid HTPB
- Binding Agent (Papi 94 - polymethylene polyphenylisocyanate)
- 4 inch diameter PVC pipe
- 1 inch diameter PVC pipe
- Cardboard
- Saw

Procedure:

1. Cut 4 inch diameter PVC pipe to a height of 6 to 12 inches
2. Cut 1 inch diameter PVC pipe to same height as previous 4 inch diameter pipe
3. Grind all pipe faces so that faces are flat and perpendicular to standing surface.
4. Place 1 inch diameter pipe into center of 4 inch PVC pipe with both pipes upright, as shown in figure 103
5. Coat 1 inch diameter pipe with anti seize compound
6. Place piping assembly onto a cardboard base
7. Ensure pipes and cardboard base assembly are rigid and taut
8. Measure and pour 172 grams of liquid HTPB into two mixing cups
9. Measure and pour 28 grams of binding agent into two mixing cups

10. Mix 100 grams of HTPB compound with the proper 86:14 ratio with the wooden mixing stick for 1 minute. Not too excessive and not too calm.
11. Pour the mixture inside space between the inner diameter of the 4 inch pipe and the outer diameter of the 1 inch pipe.
12. Repeat steps 9 and 10 with the remaining liquids
13. Place assembly into room temperature environment, and wait for 24-48 hours
14. Take a saw cut outer PVC pipe casing in half
15. Remove outer PVC casing from solid grain
16. Remove inner PVC pipe from solid grain
17. Cut grain in half vertically.
18. Visually observe any bubbles and note the distribution and frequency of air bubbles that have formed on surface. Observe and note the percentage of the fuel grain surfaces which are covered in bubbles.
19. Cut grain horizontally in the center and observe central surface bubble distribution



Figure C.1. Cut and ground PVC piping in proper mold orientations

The procedure was carried out with a mold shown in Fig. C.1. Excessive bubbles found in the mold, as shown in Fig. C.2. Bubbles are seen throughout the area of the mold. Whiter regions signify high bubble density, while the gold region signifies clear, smooth fuel compound. In this control mold, it can be seen that the surface has about 80-90 percent area of the grain compound covered in bubbles.



Figure C.2. Hardened Fuel grain control mold, bubbles are present as the white regions, where clear golden regions are absent of bubbles (marked in red)

C.0.2 Fuel Grain Casting Test Plan—Shaker Table

The solid fuel grain is an important part of the hybrid rocket engine. It contains the solid propellant, which burns in the presence of oxidizer and excessive heat. The grain is made up of solid HTPB (Hydroxyl-terminated polybutadiene) mixed with a binding agent. The HTPB must be cast and hardened into a solid grain with an even consistency, however it commonly forms bubbles in the grain. The presence of air bubbles will cause an inconsistent burn. In order to counteract this, tests are being undertaken in order to cast a grain without any air bubbles present. This particular test is done with a shaker table, in an attempt to remove air bubbles.

Calculations:

- Liquid HTPB to Binding compound (Papi 94 - polymethylene polyphenylisocyanate)
= 86 to 14
- Fuel Grain Curing Time = 24 to 48 hours
- Shaker mount frequency = 42 Hz

Supplies:

- Mixing Cups (4)
- Wooden mixing stick
- Scale
- Liquid HTPB
- Binding Agent (Papi 94 - polymethylene polyphenylisocyanate)

- 4 inch diameter PVC pipe
- 1 inch diameter PVC pipe
- Cardboard
- 6 amp Chicago Electric Reciprocating saw
- Two 2x4x2 wooden boards
- Two wood clamps

Procedure:

1. Cut 4 inch diameter PVC pipe to a height of 6 to 12 inches
2. Cut 1 inch diameter PVC pipe to same height as previous 4 inch diameter pipe
3. Grind all pipe faces so that faces are flat and perpendicular to standing surface.
4. Place 1 inch diameter pipe into center of 4 inch PVC pipe with both pipes upright, as shown in figure 103
5. Coat 1 inch diameter pipe with anti seize compound
6. Place piping assembly onto a cardboard base
7. Ensure pipes and cardboard base assembly are rigid and taut
8. Measure and pour 172 grams of liquid HTPB into two mixing cups
9. Measure and pour 28 grams of binding agent into two mixing cups
10. Mix 100 grams of HTPB compound with the proper 86:14 ratio with the wooden mixing stick for 1 minute. Not too excessive and not too calm.
11. Pour the mixture inside space between the inner diameter of the 4 inch pipe and the outer diameter of the 1 inch pipe.
12. Repeat steps 9 and 10 with the remaining liquids
13. Place wooden boards underneath and overhead of the piping assembly
14. Clamp piping assembly to Chicago electric reciprocating saw and test table using two wood clamps
15. Test to ensure assembly is tight and immobile
16. Turn on reciprocating saw to full throttle and keep it on for 30 minutes
17. Remove shaker table assembly and wait 24-48 hours for the mold to cure
18. Take a saw cut outer PVC pipe casing in half

19. Remove outer PVC casing from solid grain
20. Remove inner PVC pipe from solid grain
21. Cut grain in half vertically.
22. Visually observe any bubbles and note the distribution and frequency of air bubbles that have formed.

Setup Photographs:



Figure C.3. test stand setup of homemade shaker table



Figure C.4. Cut and ground PVC piping in proper mold orientations

Results:

Excessive bubbles found in the mold. The bubbles are forming more towards the outer circumference of the mold, however the frequency and size of bubbles are very comparable to the control model. This test has failed to produce fewer bubbles in the fuel grain mold.



Figure C.5. Cross-section of HTPB exposing bubbles (lighter areas)

C.0.3 Fuel Grain Casting Test Plan—Vacuum

The solid fuel grain is an important part of the hybrid rocket engine. It contains the solid propellant, which burns in the presence of oxidizer and excessive heat. The grain is made up of solid HTPB (Hydroxyl-terminated polybutadiene) mixed with a binding agent. The HTPB must be cast and hardened into a solid grain with an even consistency, however it commonly forms bubbles in the grain. The presence of air bubbles will cause an inconsistent burn. In order to counteract this, tests are being undertaken in order to cast a grain without any air bubbles present.

Calculations:

- Liquid HTPB : Binding compound = 86 : 14
- Fuel grain Curing time 24-48 hours

Supplies:

- Mixing Cups (4)
- Wooden mixing stick
- Scale

- Liquid HTPB
- Binding Agent*
- 4 inch diameter PVC pipe
- 1 inch diameter PVC pipe
- Cardboard
- Saw
- Vacuum Chamber

Procedure:

1. Cut 4 inch diameter PVC pipe to a height of 6 to 12 inches
2. Cut 1 inch diameter PVC pipe to same height as previous 4 inch diameter pipe
3. Face off pipes so that both faces are flat
4. Place 1 inch diameter pipe into center of 4 inch PVC pipe with both pipes upright.
5. Coat 1 inch diameter pipe with anti seize compound
6. Place piping assembly onto a cardboard base
7. Ensure pipes and cardboard base assembly are rigid and taut
8. Measure and pour 172 grams of liquid HTPB into two mixing cups
9. Measure and pour 28 grams of binding agent into two mixing cups
10. Mix 100 grams of HTPB compound with the proper 86:14 ratio with the wooden mixing stick for 1 minute. Not too excessive and not too calm.
11. Pour the mixture inside space between the inner diameter of the 4 inch pipe and the outer diameter of the 1 inch pipe.
12. Repeat steps 9 and 10 with the remaining liquids
13. Place assembly into vacuum chamber, and wait 1 hour
14. Place assembly into room temperature environment, and wait for 24-48 hours
15. Take a saw cut outer PVC pipe casing in half
16. Remove outer PVC casing from solid grain
17. Remove inner PVC pipe from solid grain
18. Cut grain in half vertically.

19. Visually observe any bubbles and note the distribution and frequency of air bubbles that have formed.

Setup Photographs:



Figure C.6. Cut and ground PVC piping in proper mold orientations (same as shaker test piping)

APPENDIX D: Structural FEA

The team ran an FEA simulation on the combustion chamber to verify structural integrity in its extreme thermal conditions, as discussed in the thermal analysis section. The corresponding figures are reproduced here.

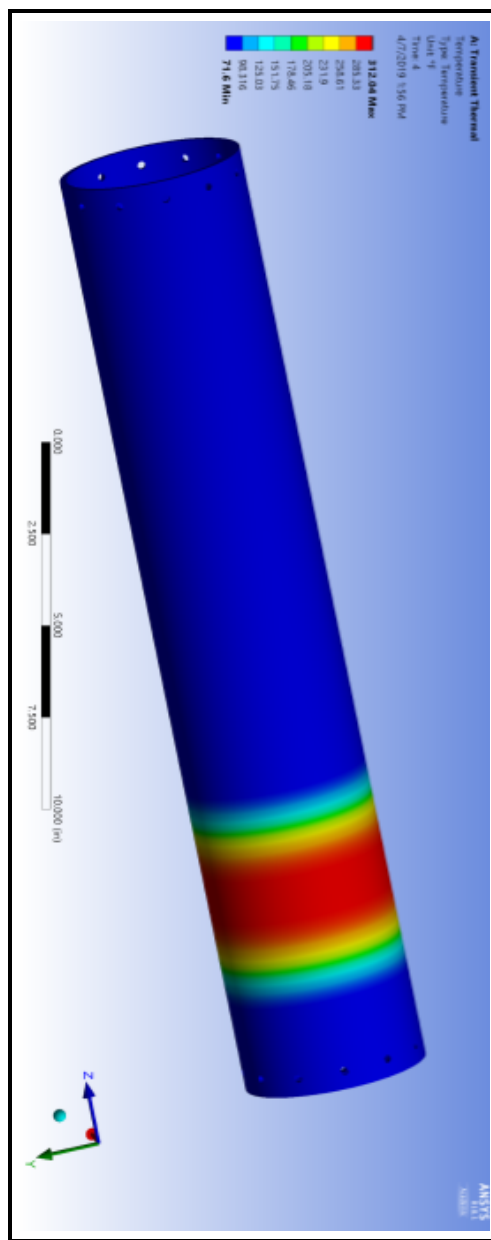


Figure D.1. Final Case Temperature Distribution on outer case surface



Figure D.2. Case Loading Conditions for Transient Structural Analysis.



Figure D.3. Final structural coupled result.

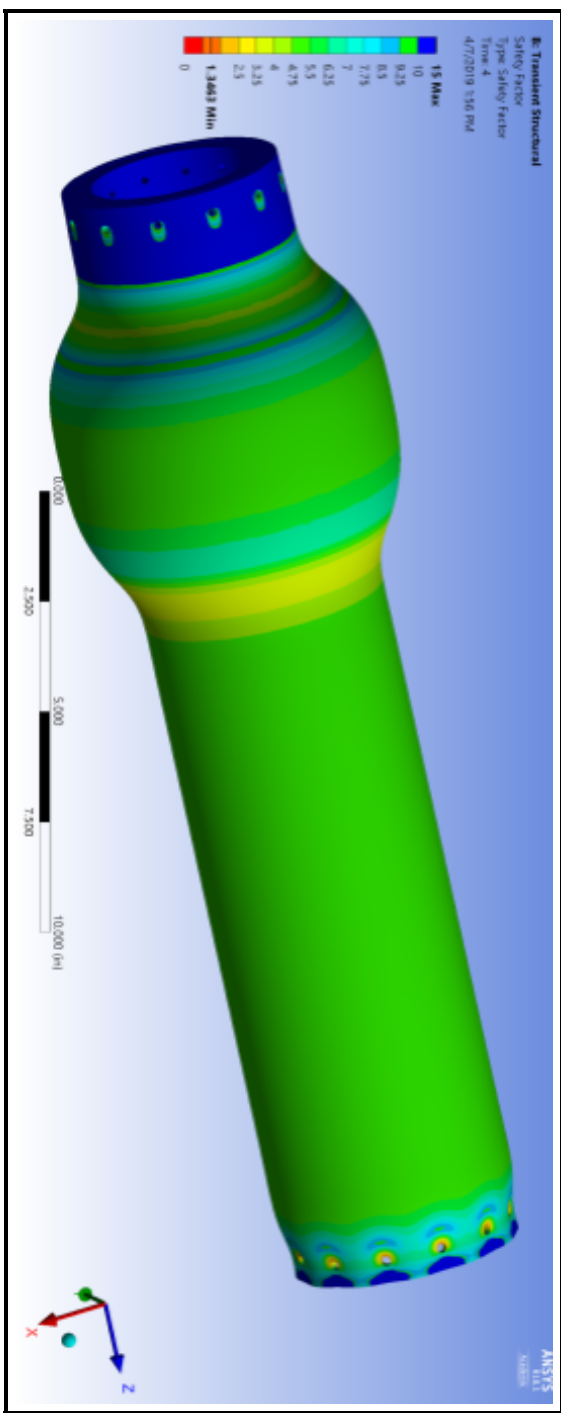


Figure D.4. Whole case structural coupled result

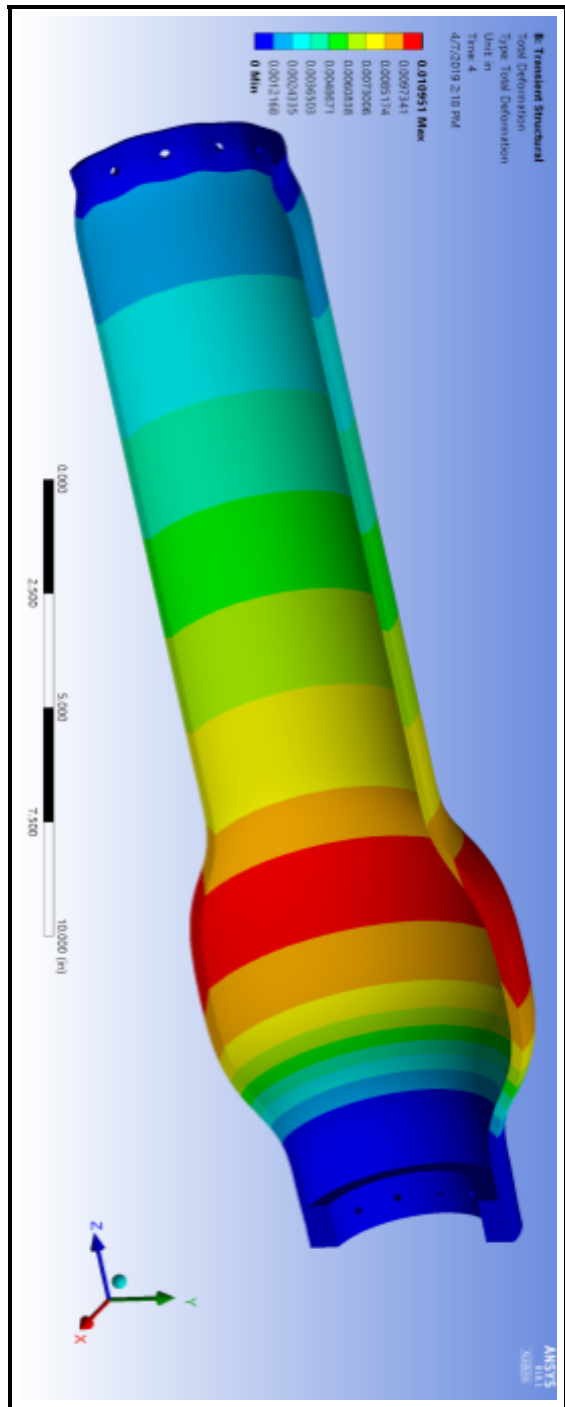


Figure D.5. Case Deformation.

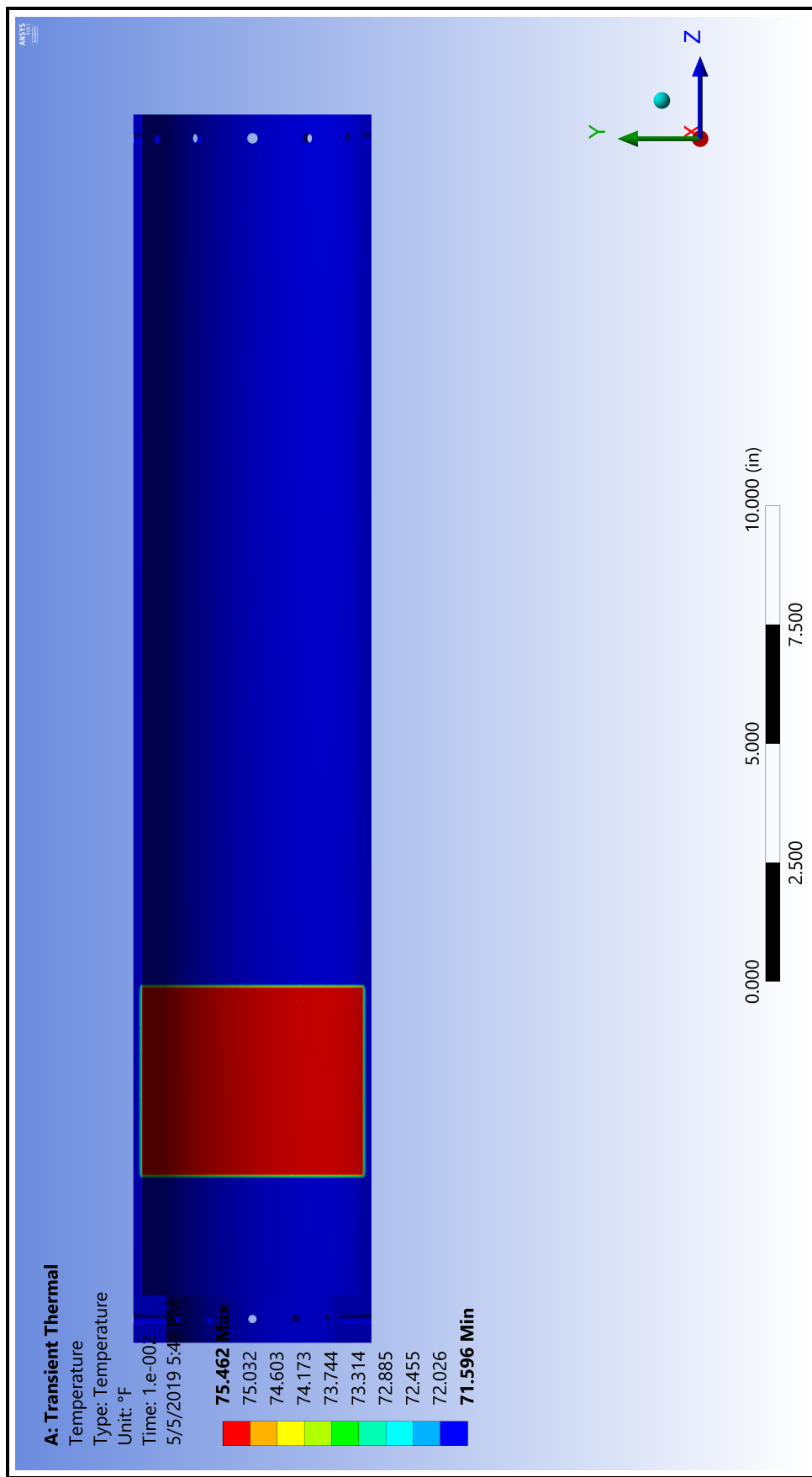


Figure D.6. Case Temperature Distribution at $t = 0\text{s}$.

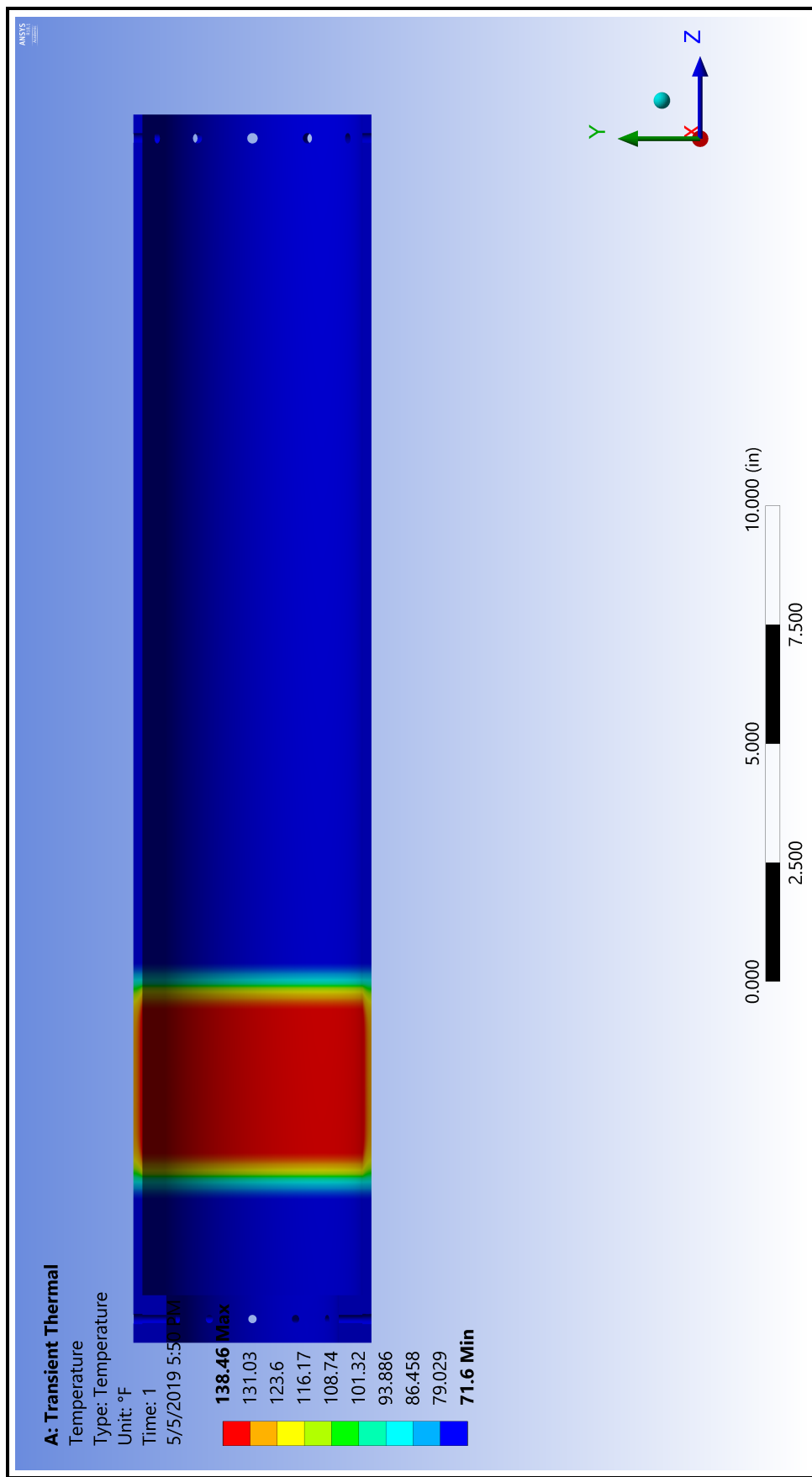


Figure D.7. Case Temperature Distribution at $t = 1\text{s}$.

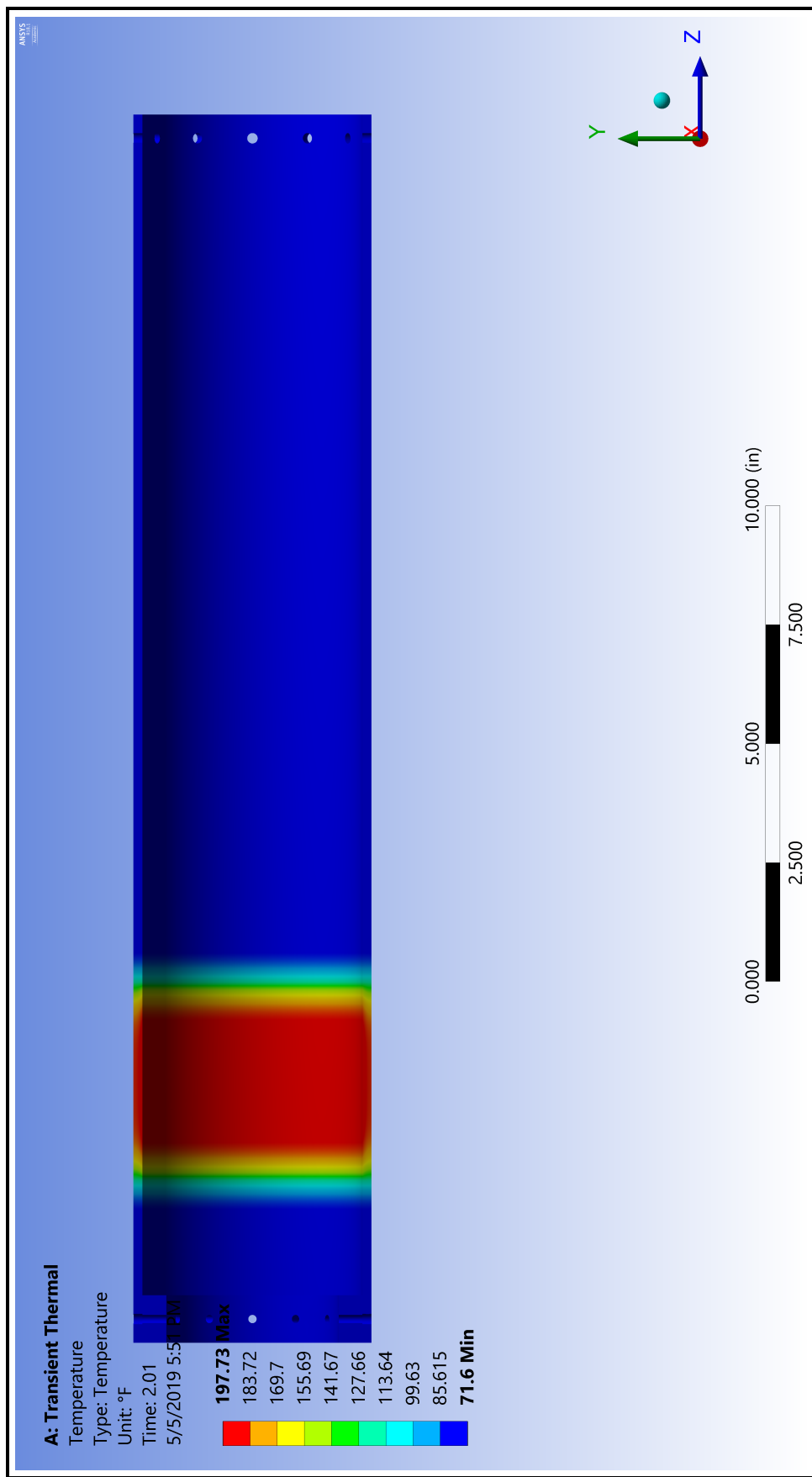


Figure D.8. Case Temperature Distribution at $t = 2\text{s}$.

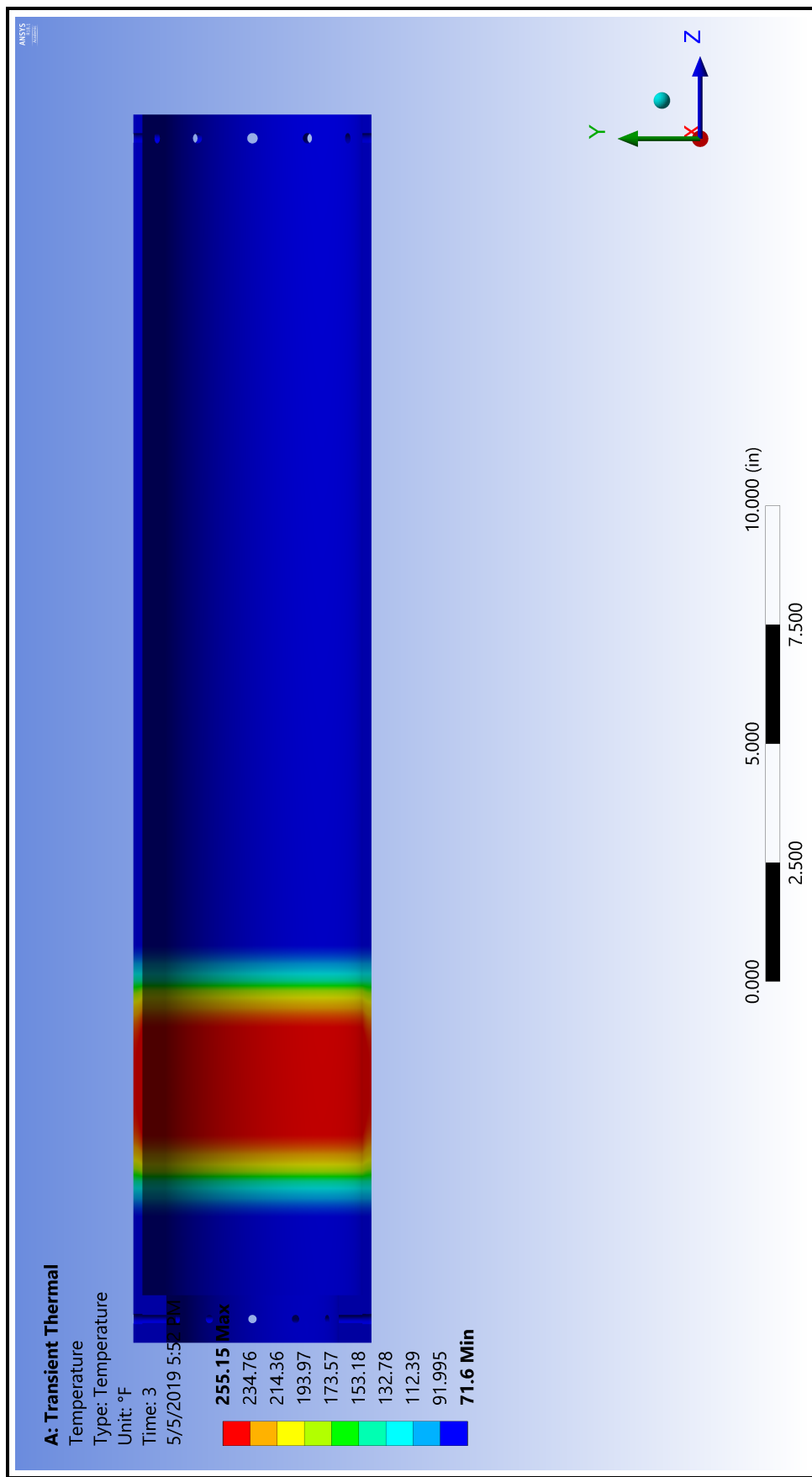


Figure D.9. Case Temperature Distribution at $t = 3\text{s}$.

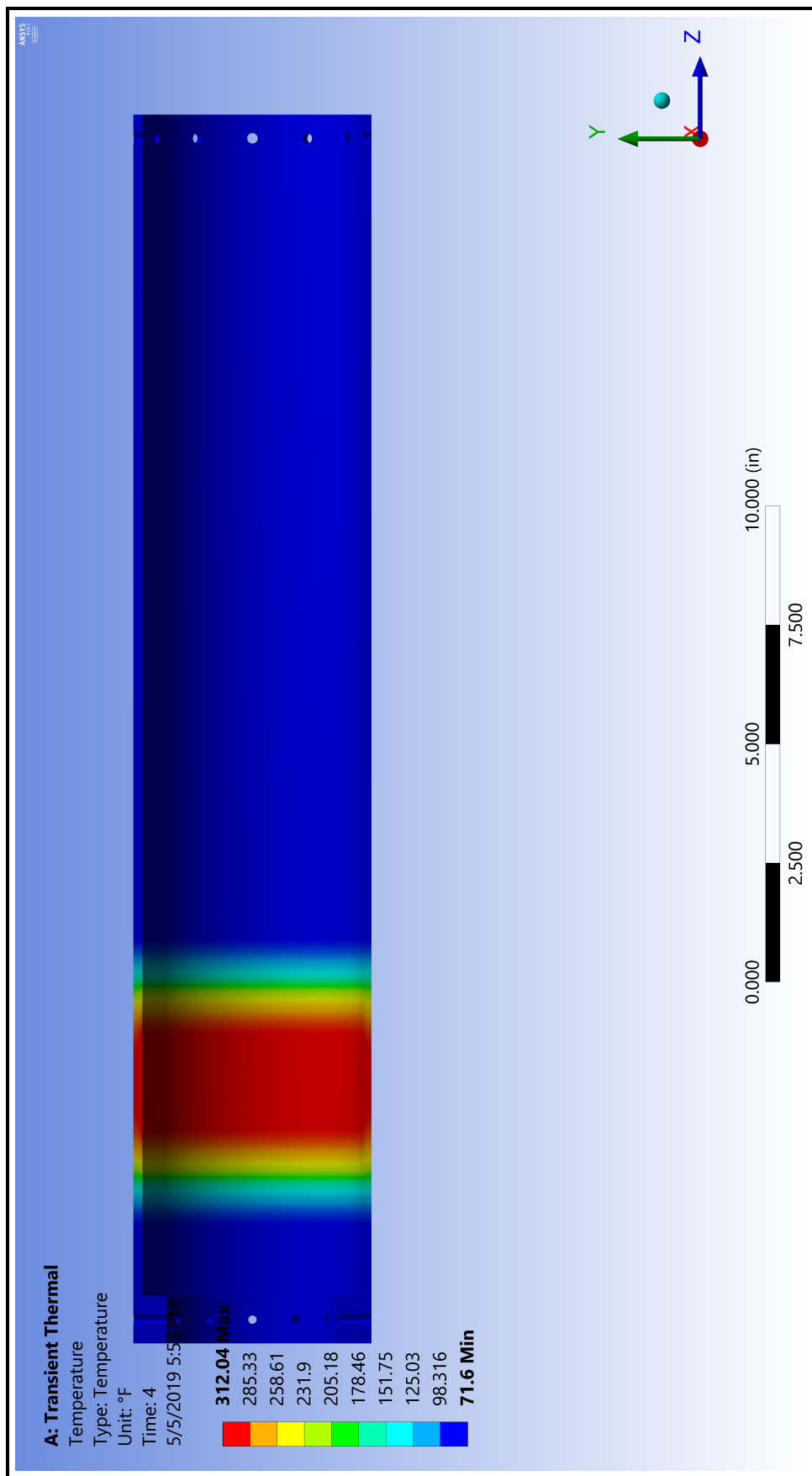


Figure D.10. Case Temperature Distribution at $t = 4$ s.

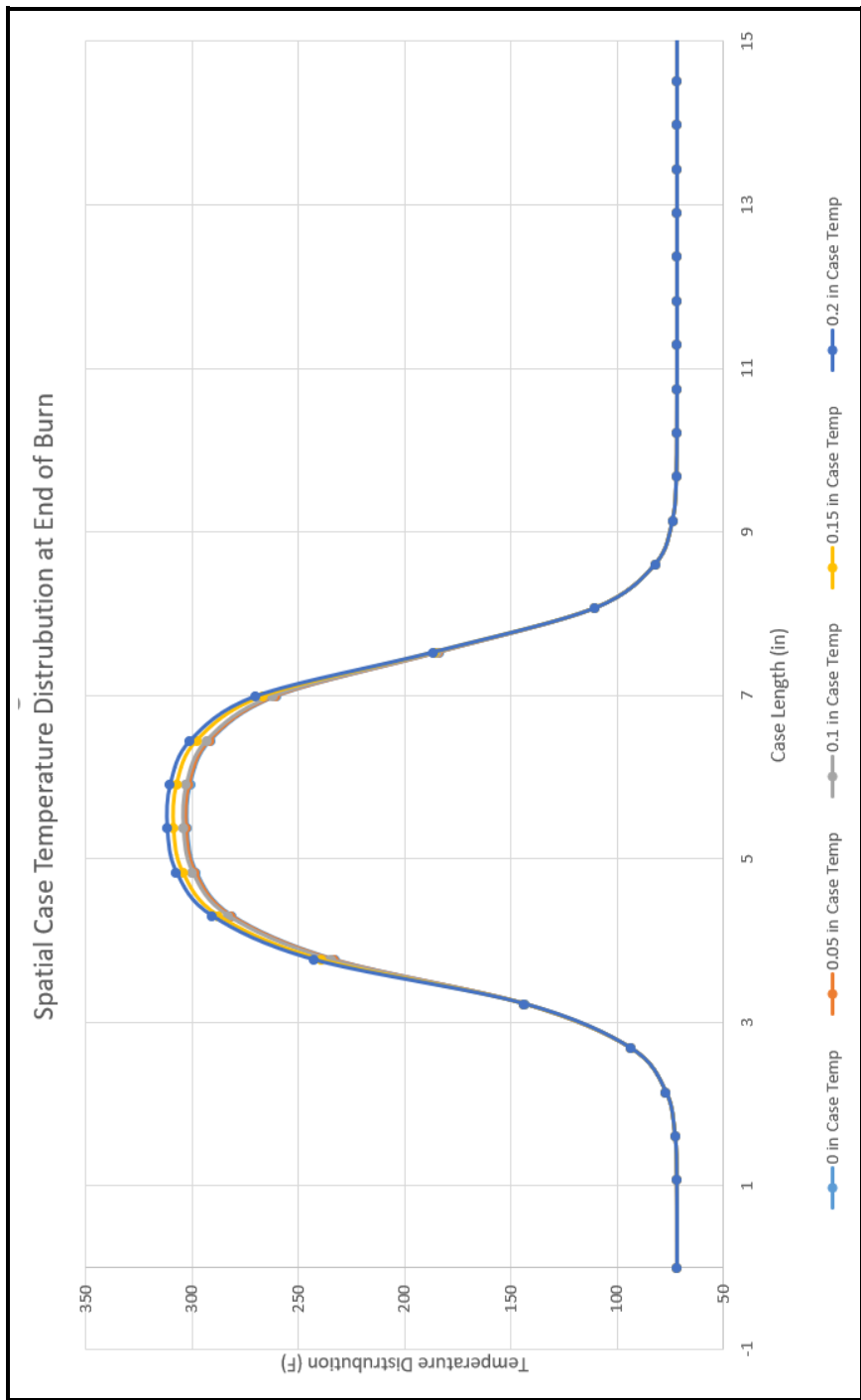


Figure D-11. Beginning at $d = 0$ in at the outer surface of the case and subsequent distributions are of 0.05 in increments until inner case is reached. Results from ANSYS simulation data

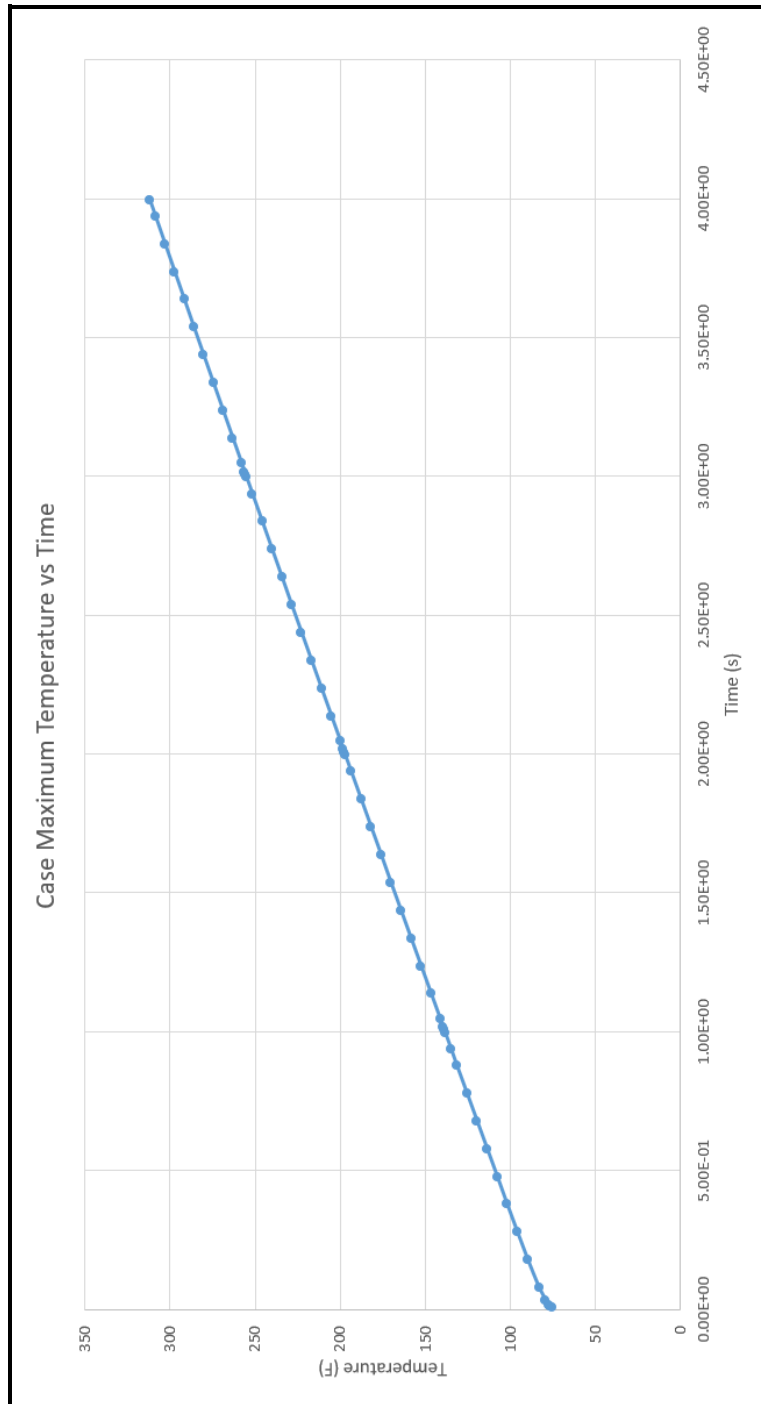


Figure D.12. The maximum temperature of the case over burn time from ANSYS simulation data.

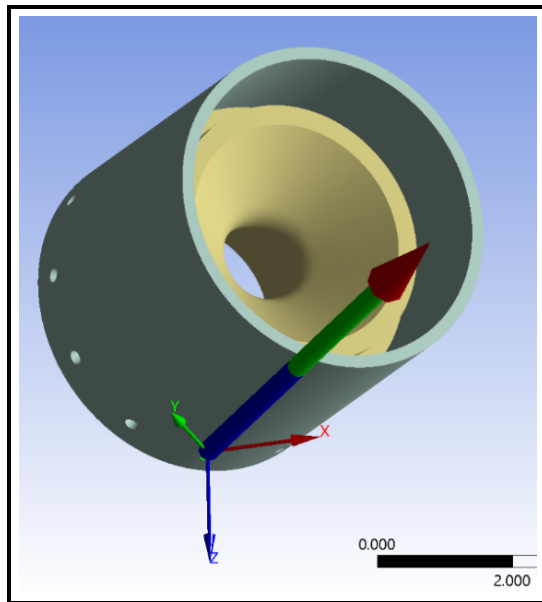


Figure D.13. Nozzle retaining ring bolt loading (CAD model courtesy of LRA)

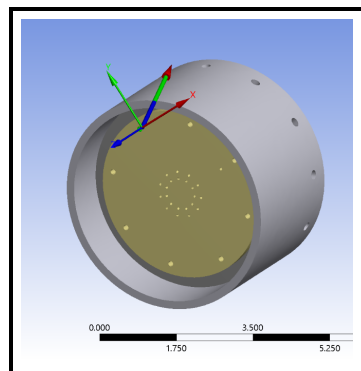


Figure D.14. Injector face bolt loading analysis (CAD model courtesy of LRA)

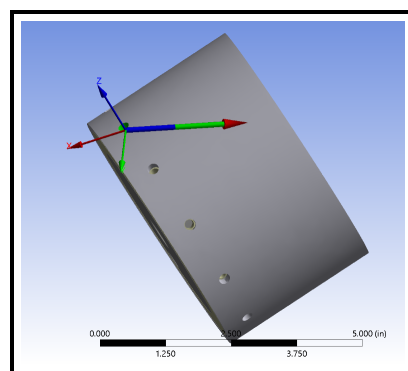


Figure D.15. Injector retaining ring loading (CAD model courtesy of LRA)

APPENDIX E: Fuel Grain Regression Calculator Results

The team created a fuel grain regression simulator to optimize the fuel grain geometry for constant thrust over its 4s burn time. The results, discussed previously in the main body of the report, are reproduced graphically here. Figs. E.1 and E.2 verified the proper operation of the program. The plans for Taurus II call for a constant thrust curve; that of Fig. E.3 is our best design to date.

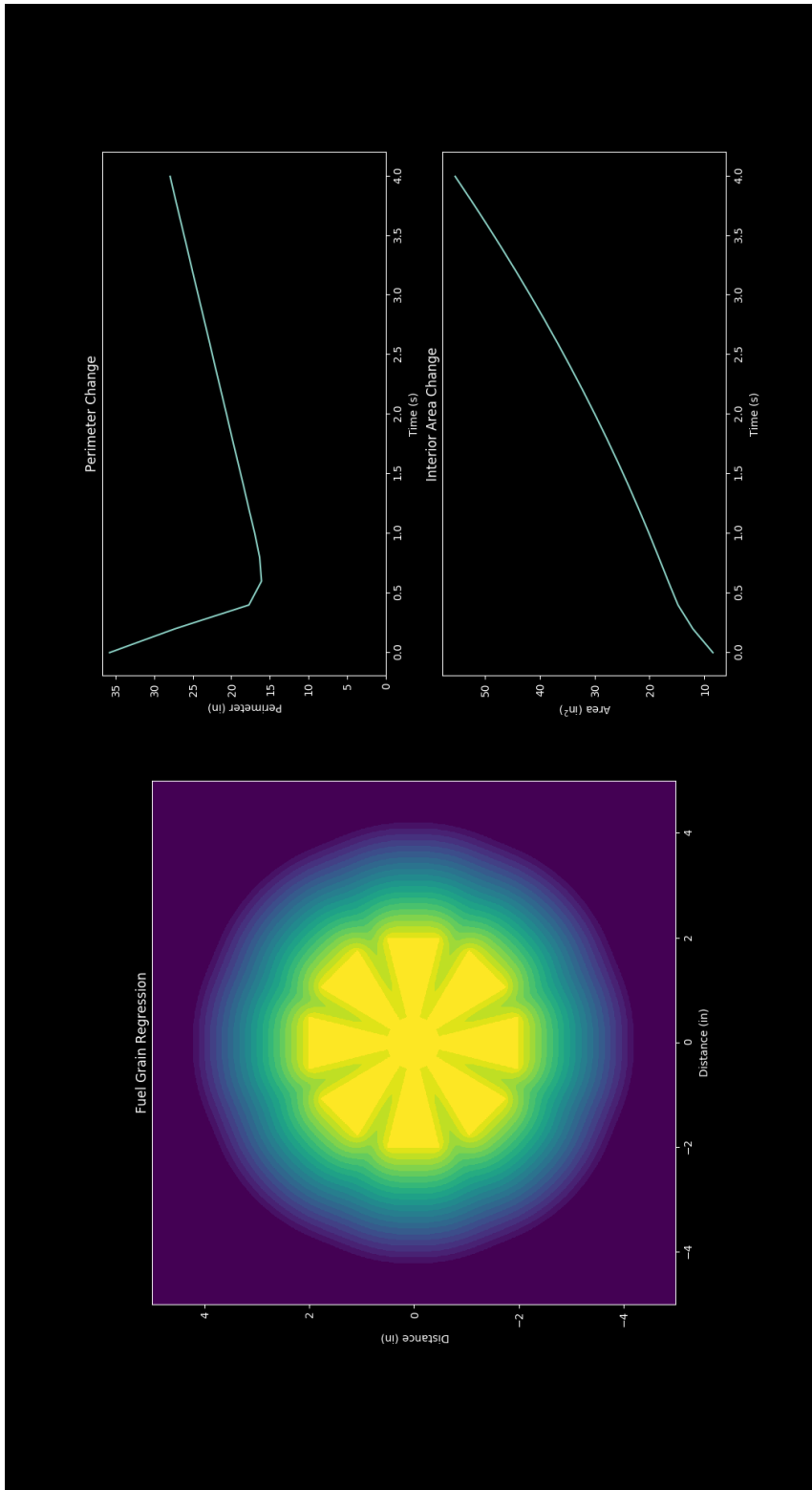


Figure E.1. A sample analysis of a fuel grain. The original cross-section of the fuel grain is solid save for the yellow star in the center. During combustion, the fuel burns into the green, then blue areas, creating the perimeter and area curves shown on the right. Note the perimeter rises and falls at different times during combustion (the interior area, of course, always increases, as fuel does not un-combust).

E-2

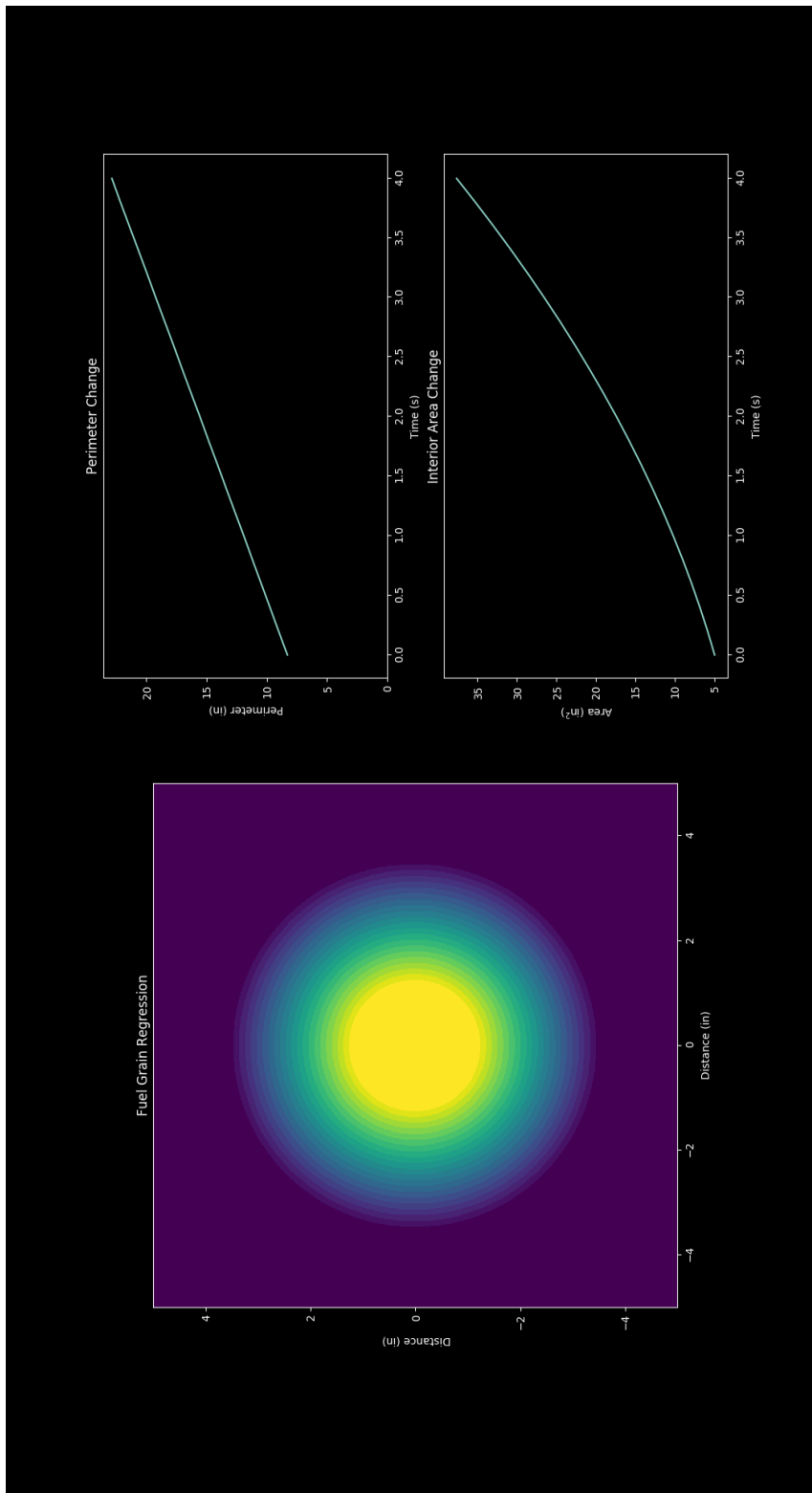


Figure E.2. A basic circle geometry. As expected, perimeter increases linearly with diameter increase, while area rises quadratically. This is useful as a test case and, indeed, the results of the calculator agree with geometric calculations for area and perimeter.

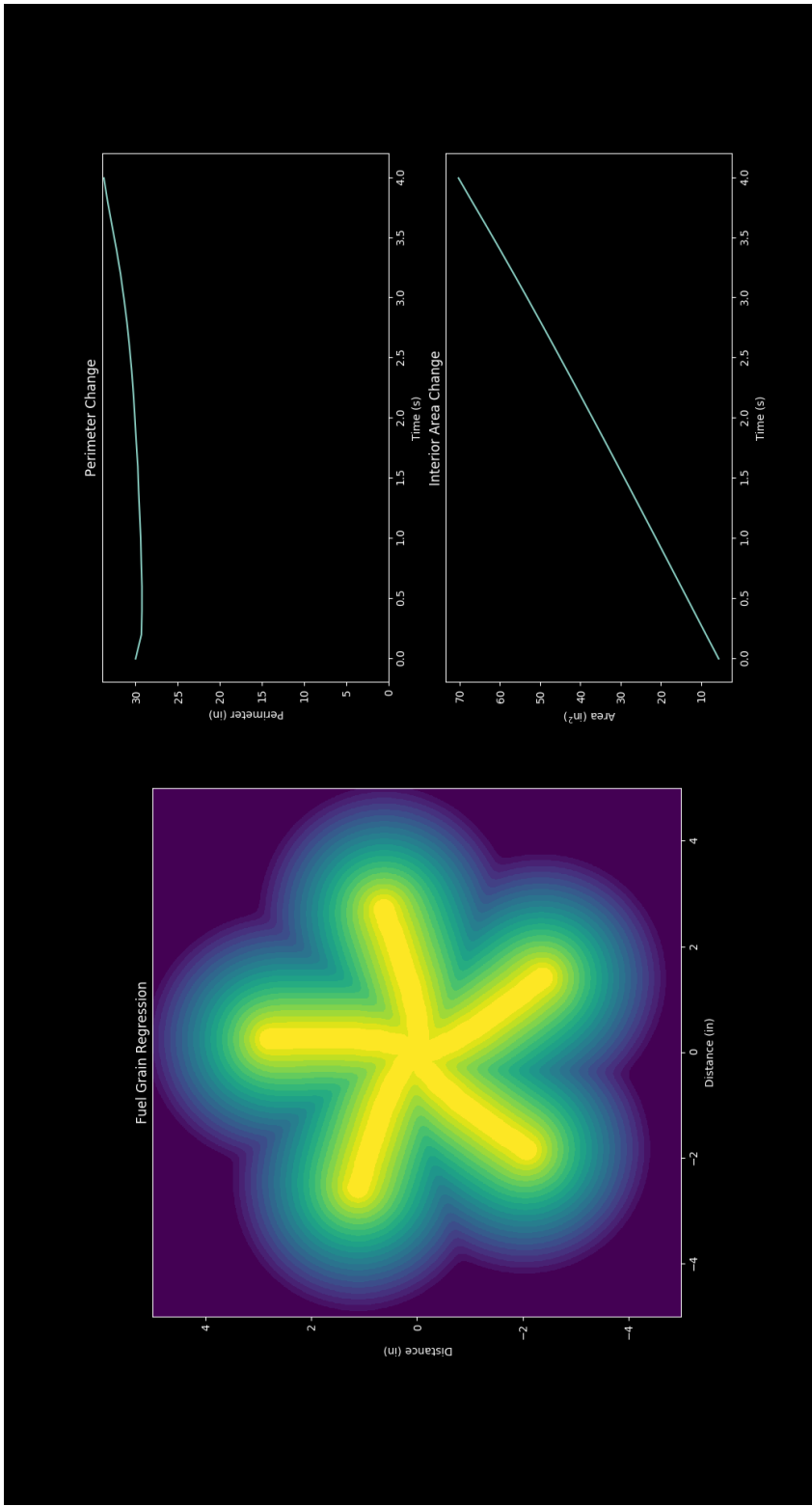


Figure E.3. A simple star of lines turns out to provide a near-constant perimeter. Tests (not shown here) imply the exact thrust curve depends on the width of each arm and the number of arms; fewer arms create a decreasing perimeter; more reverse the effect. A five-pointed star seems to be near the equilibrium for reasonable amounts of interior area. We do note that such thin channels in the original fuel grain require reasonably advanced manufacturing.

E-4

APPENDIX F: Fluid Geometry

F.1 Nozzle Output Results

Nozzle Design

- Simple conical converging-diverging nozzle
- Converging 45 [deg]
- Diverging 20 [deg]
- Material: ACF-10Q Graphite (14,000 psi flexural strength)

Calculated Parameters

- Chamber Temperature (R) = 6103.09
- Throat Radius (in) = 0.60
- C
- (ft/s) = 5310.04
- Exit Mach Number = 2.79
- Isp = (247.876736736391, UnderExpanded Pe=16.2972)
- Chamber Molecular Weight = 26.25

Input Parameters

- Chamber Pressure (psi) = 500
- *Expansion Ratio = 5.25
- Mass Flow Rate (lb/s) = 3.63
- Mass Ratio = 6.3

- Ambient Pressure (psi) = 14.7

Outputs

- Exit Velocity ft(s) = 7528.28
- Thrust (lbf) 848.68

Combustion Chamber Code Outputs

Input Parameters

- Ceramic Thermal Conductivity (BTU/(hr-F-ft)) = 0.928
- Ceramic Thickness (in) = 0.004
- Ablative Thermal Conductivity (BTU/(hr-F-ft)) = 0.696
- Ablative Thickness (in) = 0.25
- Case Initial Temperature (R) = 530.67
- Case Specific Heat (BTU/(hr-F-ft)) = 0.215

Combustion Chamber Geometry

- Combustion Chamber Length (in) = 4
- Combustion Chamber Surface Area (in^2) = 58.11
- Combustion Chamber Volume (in^3) = 17.01

Output Parameters

- Chamber Heat Transfer Coefficient (Btu/ $\text{in}^2\text{-s-F}$) = 0.00113
- Combustion Chamber Heat Flux (Btu/ $\text{in}^2\text{-s}$) = 18.78
- Combustion Chamber Temperature (R) 6103.09
- Casing Final Temperature (R) = 744.577
- Chamber Diameter (in) = 3.523
- Chamber Length (in) = 7.646